August 2014

Multi-Periodic Climate Dynamics: Spectral Analysis of Instrumental, Short- and Long-length Proxy Temperature Records

Michael David Madsen
University of Wisconsin-Milwaukee

MULTI-PERIODIC CLIMATE DYNAMICS: SPECTRAL ANALYSIS OF INSTRUMENTAL, SHORT- AND LONG-LENGTH PROXY TEMPERATURE RECORDS

by

Michael David Madsen

A Thesis Submitted in

Partial Fulfillment of the

Requirements for the Degree of

Master of Science

in Mathematics

at

The University of Wisconsin-Milwaukee

August 2014

ABSTRACT

MULTI-PERIODIC CLIMATE DYNAMICS: SPECTRAL ANALYSIS OF INSTRUMENTAL, SHORT-LEGNTH PROXY TEMPERATURE RECORDS, AND LONG-LENGTH PROXY TEMPERATURE RECORDS

by

Michael David Madsen

The University of Wisconsin-Milwaukee, 2014
Under the Supervision of Professor Anastasios Tsonis

Analyzing 26 short-length (less than 3000 years) instrumental and proxy temperature records and five long-length (greater than 3000 years) proxy temperature records using Discrete Fourier Transform has shown that as the length of significant periods increase in the time domain then so does the power at which the period is observed. A t-test verifies that a positive correlation exist between the length of the significant periods and the power with a confidence level of $\propto > 0.05$. Significant frequencies with period greater than 30 years are confirmed using Monte Carlo simulations, which were created using a nonlinear approach known as fractional Brownian motion (FBM). While completing the spectral analysis it was observed in the spectral analysis is an absence of significant periods between about 1000 years and 20 000 years. Also, wavelet analysis of all short-length temperature records turned up no significant findings.

TABLE OF CONTENTS

LIST OF FIGURES

LIST OF TABLES

I. Introduction

Spectral analysis of multi-periodic climate dynamics have been completed in past. However, only a handful of temperature records have been analyzed at one time in previous studies, as in a publication by H. J. Lüdecke et al. (Lüdecke et al., 2013). Here H. J. Lüdecke et al. only looked six "long-term" instrumental and one proxy temperature record for their analysis. Their goal was to show that the climate dynamics are governed at present by periodic oscillations. While their goals were reached, their sample size for the spectral analysis was limited to only two temperature records, one of which was an mean of the six "long-term" instrumental temperature records and the other being used as only as a comparison, not for actual analysis. In order to complete a better view of multi-periodic climate dynamics, more temperature records need to be analyzed. For this study the same six instrumental temperature records and the one proxy temperature record where reanalyzed as well as 19 other short-length (less than 3000 years) and 5 long-length (greater than 3000 years) proxy temperature records where analyzed to determine if the hypothesis, that as the period length increase in climate dynamics than so does the power at which that period exist, is found valid. Also, each temperature record was analyzed using wavelet analysis to discover if there were any characteristics of the Feigenbaum universal scenario of transition to chaos by a cascade of subharmonics, for nonlinear, dissipative systems with energy input (Feigenbaum, 1978, 1983).

II. Data

Twenty different reconstructed short-length proxy temperature records and six instrumental temperature records as well as five long-length proxy temperature records, four of which are ice-core reconstructed temperature records and the other reconstructed temperature record being from marine benthic oxygen isotopes, were analyzed in this study. The reconstructed proxy temperature records range in length, location, and methods including sediment thickness and pigment, tree-ring thickness, varve thickness, stalagmite thickness and isotopes, documentary data, ice core samples, marine benthic oxygen isotopes, and multi-proxy reconstruction while the instrumental temperature records were all located in central Europe and only ranged from 231 year-long temperature records to 247 year-long temperature records and are monthly means records. The length in all the temperature records range from the longest being a 1,069,900 years (-1,067,900–2000 AD) marine benthic oxygen isotopes reconstruction to the shortest being a 231 year (1781-2011 AD) instrumental record from Munich, Germany. All short-length temperature records were converted to yearly means and all long-length temperature records were converted to 50 years, 100 years, or 500 years for the application of discrete Fourier transform. This dictates that the six instrumental records were converted from monthly means to yearly means and that two short-length temperature records (Iceberg, Alaska and Spannagel Cave, Europe) and three of the long-length temperature records (EPICA Dome C, Antarctica; GISP2 ice core, central Greenland; and Vostok, Antarctica) were interpolated to fill in missing yearly means or to create a fixed yearly/multi-yearly interval. The details of the records used in this paper are

in table 1 and as follows: Laguna Aculeo, Chile, summer mean sediment pigments, data in figures 1 & 2 (856–1997 AD) (Von Gunten et al., 2009); Baffin Island, Canada, summer mean sediment thickness, data in figures 3 & 4 (752–1992 AD) (Moore et al., 2003); Canadian Rockies, Canada, summer mea tree-ring thickness, data in figures 5 & 6 (950–1994 AD) (Luckman et al., 2006); Firth, Alaska, summer mean tree-ring thickness, data in figures 7 & 8 (1073–2002 AD) (Anchukaitia et al., 2013); Iceberg Lake, Alaska, annually varve thickness, data in figures 9 & 10 (442–1998 AD) (Loso, 2008); Gulf of Alaska, summer mean tree-ring thickness, data in figures 11 & 12 (724–1999 AD) (Wilson et al., 2007); Idaho, USA, annually July mean tree-ring thickness, data in figures 13 & 14 (1135–1992 AD) (Biondi et al., 2006); North Andes, South America, annual mean tree-ring thickness, data in figures 15 & 16 (1640–1987 AD), South Andes, South America, annual mean tree-ring thickness, data in figures 17 & 18 (1640–1993 AD) (Villalba et al., 2006); Beijing, China, summer mean stalagmite thickness, data in figures 19 & 20 (-665–1985 AD) (Tan et al., 2003); Central Europe, annual mean documentary data, data in figures 21 & 22 (1005–2001 AD) (Glaser and Riemann, 2009); China, annual multi-proxy reconstruction, data in figures 23 & 24 (1000–1950 AD) (Shi et al., 2012); Cold Air Cave, South Africa, 5-year smoothed annual stalagmite isotope, data in figures 25 & 26 (1635–1993 AD) (Sundqvist et al., 2013); European Alps, summer mean tree-ring and sediment thickness, data in figures 27 & 28 (1053–1996 AD) (Trachsel et al., 2012); Lake Silvaplana, Switzerland, summer mean visible reflectance spectroscopy of lake sediment, data in figures 29 & 30 (1175–1949 AD) (Trachsel et al., 2010); Slovakia, Europe, summer mean tree-ring, data in figures 31 & 32 (1040–2011 AD)

(Büntgen et al. 2013); Sweden, Europe, summer mean tree-ring, data in figures 33 & 34 (1107–2007 AD) (Gunnarson et al., 2011); Tornetrask, Sweden, annual tree-ring, data in figures 35 & 36 (500–2004 AD) (Grudd, 2008); West Qinling Mts., China, annual tree-ring, data in figures 37 & 38 (1500–1995 AD) (Yang et al., 2013); Paris, France, monthly mean instrumental, data in figures 39 & 40 (1764–2000 AD) (Météo France, 2012); Hohenpeisenenberg, Germany, monthly mean instrumental, data in figures 41 & 42 (1781–2013 AD) (CRU, 2012); Kremsmunster, Austria, monthly mean instrumental, data in figures 43 & 44 (1767–2013 AD) (Auer et al., 2007); Munich, Germany, monthly mean instrumental, data in figures 45 & 46 (1781–2011 AD) (DWD, 2012); Prague, Czech Republic, monthly mean instrumental, data in figures 47 & 48 (1771–2013 AD) (CHMI, 2012); Vienna, Austria, monthly mean instrumental, data in figures 49 & 50 (1775–2013 AD) (CRU, 2012); Spannagel Cave, Europe, stalagmite thickness, data in figures 51 & 52 (-9–1935 AD) (Mangini et al., 2005); Dome Fuji, Antarctica, Ice Core, data in figures 55 & 56 (-339500–750 AD) (Kawamura et al., 2007); EPICA Dome C, Antarctica, Ice Core, data in figures 57 & 58 (-800,000–1900 AD) (Jouzel et al., 2007); GISP2 ice core, central Greenland, Ice core, data in figures 59 & 60 (-48000–1850 AD) (Alley, 2004); Global 1Ma Temperature, marine benthic oxygen isotopes, data in figures 61 & 62 (-1067900–2000 AD) (Bintanja et al., 2005); Vostok, Antarctica, Ice Core, data in figures 63 & 64 (-470766–2000 AD) (Petit et al., 1999).

III. Method

In this study, we used the simple method of discrete Fourier transform (DFT) as our method for spectral analysis. DFT converts finite, equal spaced time domain samples, temperature records, into a finite combination of complex sinusoids ordered by their frequencies. In principle, unequal time steps for DFT is not applicable, so each temperature records with unequal time steps is converted to have a discrete time step of one year, for all short-length temperature records, and either 50 years, 100 years, or 500 years for all long-length temperature records by either monthly averaging or interpolating. The six instrumental temperature records were all monthly averages, so each month in the calendar year was averaged to give us our yearly time step. The two short-length temperature records and three long-length temperature records that have unequal time steps and missing yearly data were all interpolated using a piecewise cubic spline interpolation function in Matlab® (interp1) (Matlab®, 2012b). However, interpolating can result in enhancing lower frequencies and reducing higher frequency components (Schulz and Mudelsee, 2002). To verify that our interpolation have little to no effect on the frequency components, our interpolated temperature records' DFT spectral analysis are compared to the spectral analysis using the Lomb-Scargle periodogram method. For Iceberg Lake, Alaska, 20 missing yearly data points were interpolated in and as an outcome no significant difference in peak frequency or intensity were observed. As for Spannagel Cave, Europe, the uneven time increments were interpolated to have a yearly time step and as an outcome no significant difference in peak frequency occurred but a difference in

peak intensities occurred between the two methods. Because the largest time steps for Spannagel Cave, Europe lies between 90 BC and 500 AD, this section of the temperature record is omitted and the comparison is carried out again. As a result, we find that both peak frequency and intensity are comparable between the two methods using this shortened interpolated Spannagel Cave, Europe time series. The three interpolated long-length proxy temperature records, EPICA Dome C, Antarctica; GISP2 ice core, central Greenland; and Vostok, Antarctica, also underwent the same comparison, and as a result it is fond that both peak frequency and intensity are comparable between the two methods.

Each temperature record used in this study was first detrended using the Matlab® function (detrend), then in order to obtain more frequency steps in the DFT spectral analysis, zero padding was applied to both ends the temperature records to create temperature records of equal length of N=10000 time steps. Each temperature records were centered within the zero padding. Each temperature records then underwent the discrete Fourier transform using the fast Fourier transform function in Matlab® (fft). The output of this function was a combination of complex sinusoids in the form $A + Bi$, where A and B are a pair of harmonic predictors which can be found using:

$$A_k = \frac{2}{N}\sum_{i=1}^{N} y_i \cos\frac{2\pi k i \Delta t}{T}$$

$$B_k = \frac{2}{N}\sum_{i=1}^{N} y_i \sin\frac{2\pi k i \Delta t}{T}$$

$$for:\ k = 1, \frac{N}{2} - 1$$

$$A_{\frac{N}{2}} = \frac{1}{N}\sum_{i=1}^{N} y_i \cos\frac{\pi N i \Delta t}{T}$$

$$A_0 = \frac{1}{N}\sum y_i$$

$$B_0 = B_{\frac{N}{2}} = 0$$

where Δt is the time interval, $y_n = y(t_n)_{\ n=1,N}$, and $T = N\Delta t$. To find the variance associated with a given pair of harmonic predictors (C_k):

$$C_k = \frac{{A_k}^2 + {B_k}^2}{2}$$

C_k gives us the power values for the power spectrum. The power values for each spectrum were then normalized by dividing by the area comprised by the whole spectrum. For this to happen it first must be pointed out that by using this method only half of the spectrum is retrieved as the second half is just a mirror image of the first half, so in order to be able to normalize each spectrum by dividing by the area of the whole spectrum we must double the area of the first half of the spectrum. And as the focus of this study is on climate periodicity, each graph only has a frequency limit of 0.04 $year^{-1}$ or 25 years.

In order to obtain significant peaks within the DFT power spectra, a 95% confidence level is applied to the spectra. For this study a 95% confidence level was established by using 1000 Monte Carlo synthetic runs using fractional Brownian motion (FBM). FBM is a nonlinear approach to create Brownian motion with a given Hurst exponent. Similar to the regression coefficients used in the red noise method, the Hurst Exponent is used as a measure of long-term memory of a temperature records (persistence). The Hurst Exponent can vary between 0 and 1, with the range

between 0.5-1 indicates persistence behavior while range between 0-0.5 indicates anti-persistence behavior. A Hurst Exponent of δ=0.90 (which if found in the Spannagel Cave, Europe time series) represents high persistence within a time series. First, in order to use FBM, each temperature records must be examined to verify that they are fractal. For this verification, we used the rescaling range analysis (method listed below in equations) (Feder, 1988). As the graph for each temperature record shows, all of the temperature records used in this study are fractals. Once each temperature record is found to be fractal, the Hurst exponent is calculated. To calculate the Hurst exponent of a time series:

$$y_n = y(t_n)$$

where:

$$n = N, \frac{N}{2}, \frac{N}{4}, \frac{N}{6}, \ldots$$

with the last term in *n* being greater than two. First, find the mean of the time series:

$$M_n = \frac{1}{n}\sum_{i=1}^{n} y_i$$

Then calculate the deviations from the mean:

$$x_1 = y_1 - M_n$$

$$x_2 = y_2 - M_n$$

$$\ldots$$

$$x_n = y_n - M_n$$

Next, calculate the cumulative sums:

$$Z_1 = x_1$$

$$Z_2 = x_1 + x_2$$

…

$$Z_n = \sum_{i=1}^{n} x_i$$

Compute the range:

$$R_n = \max[Z_n] - \min[Z_n]$$

Compute the standard deviation:

$$S_n = \sqrt{\frac{1}{n}\sum_{i=1}^{n}(y_i - M_n)^2}$$

The rescaling range $\frac{R_n}{S_n}$ can be calculated over all partial time series of length n. It is then used to estimate the Hurst exponent (H).

$$\frac{R_n}{S_n} = Cn^H$$

Where C is a constant. From here:

$$\log\left(\frac{R_n}{S_n}\right) = \log(C) + H\log(n)$$

So, by finding the "line of best fit" (slope) between $\log\left(\frac{R_n}{S_n}\right) vs \log(n)$ we can calculate the Hurst exponent H, which is the slope.

After calculating the Hurst exponent for each time series, we can create the 1000 Monte Carlo synthetic runs using the synthesize fractional Brownian motion function in Matlab® (wfbm). However, the synthesize fractional Brownian motion function only returns the fractional Brownian motion signal, so the differences in the signal's individual points must be found to get back to the fractional Brownian motion. This is done 1000 times to create the 1000 Monte Carlo synthetic runs for

each time series. These 1000 synthetic temperature records undergo the same DFT as the original temperature records and a 95% confidence level is found from the power spectrum of these synthetic DFT using the 95 percentile of the outcomes.

IV. Results

The results of the DFT analysis for the temperature records are shown in the power spectrum along with the 95% confidence level for each time series (figures 2,4,6... 52). Significant peaks occur whenever the spectral analysis is greater than the 95% confidence level. Of the 26 short-length temperature records that were analyzed in this study, all but five (Hohenpeisenberg, Germany; Kremsmunster, Austria; Munich, Germany; Prague, Czech Republic; Vienna, Austria) experienced at least one significant peak with 122 significant peaks in total. Again, because we are interested in climate dynamics, the minimum period length for this study was set at 30 years and no maximum period, however the maximum period length able to be resolved is that of the length of the temperature record itself. Significant peaks of short-length temperature records range from 30 years to 910 years, with a majority being between 30 and 100 years (about 56%).

The results of the significant peaks for all short-length temperature records are all plotted on the same graph verse the power at which the peak experienced. The results are in figure 53 along with the line of best fit. As it can be seen there is a positive correlation with the length of period and the power at which those periods occur. This would imply that longer periods would display a higher power. However, it must be tested to verify that there is a positive relationship. For this, we conducted a linear regression t-test to determine whether the slope of the regression line differs significantly from zero or in other words to determent if there is a positive correlation between period length and power level. First we state our null hypothesis and alternative hypothesis:

$$H_0: M = 0$$

$$H_a: M > 0$$

where M is the slope of the linear regression line. For this analysis, the significance level is $\alpha = 0.05$. To apply the linear regression t-test, we need to calculate the standard error of the slope, the slope of the regression line, the degrees of freedom, the t-score test statistic, and the P-value of the test statistic. The standard error of the slope can be calculated by:

$$SE = \sqrt{\frac{\frac{1}{n-2}\sum_{i=1}^{n}(y_i - \hat{y}_i)^2}{\sum_{i=1}^{n}(x_i - \bar{x})^2}}$$

In this case the standard error of the slope is $SE = 0.010951$. The slope of the regression line:

$$y = 0.18912x + 7.1484$$

In this case is $M = 0.18912$. The degrees of freedom are:

$$DF = n - 2$$

Since $n = 122$, the degrees of freedom is $DF = 120$. The t-score can be found by:

$$t = \frac{M}{SE}$$

Which gives us a t-score of $t = 17.05$. From here we can find that the p-value is $p > 0.00001$. This result is significant at a confidence level of $\propto > 0.05$. This mean that we reject the null hypothesis and that there is a positive relationship between the period length and the power intensity of the spectrums.

What this means is that if we look at the long-length temperature records we would expect to see high power among the significant peaks. By looking at figure 54

(which include all significant peaks from all temperature records) we find that a linear model hold true for increased length of period. This implies that there is an increase in power density as the length of periodicity is increased.

An interesting find from this study is that there appears to be a gap in the periodicity in which no significant peaks occur between about 1,000 years and 20,000 years. While very few of the short-length temperature records have lengths longer than 1000 years, the long-length temperature records have more that enough data points to be able to resolve this area covered by the gap, yet none of them have any significant peaks within this gap. This is most apparent in the spectral analysis of GISP2 ice core, central Greenland (figure 60). The significant peak on the left side of the spectrum has a period of about 40000 years while the significant peak on the right is about 1000 years. Note that there exist no significant peaks within this range for this graph. This is what appears on all long-length temperature record spectral analysis done in this study. This would suggest that there is nothing that has a significant effect on the dynamics of the climate between the 1000 years oscillations, which indications point that these oscillations are due to intrinsic dynamics of the Earth yet external causes for periodic dynamics can't be ruled out (Lüdecke et al., 2013), and the known 20 000 year, 40 000 year, and 100 000 year climate periods that are due to astronomical forcings.

V. Wavelet Analysis

Each short-length temperature records also underwent a wavelet analysis to determine if any shift in the dominant period occurred within the time series. The main goal of this was to determine if shifts of the subharmonic are characteristics of the transition from periodic to chaotic oscillations of a dynamic system through period doubling like that found in the wavelet analysis of Spannagel Cave, Europe (Figure 84). By looking at all 26 wavelet analyses (figures 65-90), only three temperature records experience subharmonic shifting characteristics that would suggest transition from periodic to chaotic oscillations including Spannagel Cave, Europe (the other two being Laguna Aculeo, Chile, figure 76 and Slovakia, Europe, figure 80). With no commonality amongst a majority of the wavelet analysis it can be determine that there is no global shifts of the subharmonic leading to chaotic oscillations. There does not appear to be any commonality present amounts a majority of the wavelet analysis that seams significant.

VI. Conclusion

Analyses of more temperature records are needed to further examine multi-periodic climate dynamics through the use of spectral analysis. This study only looked at 26 short-length temperature records and only five long-length temperature records. With the more temperature records used for analysis, the more defined the relationship between increase period length and increased power should become. With more long-length temperature records, the more defined the gap between about 1000 years and 20 000 year periods should become. Also, it still needs to be examined to what are the causes of all of these significant periods within the climate dynamics. While some causes are know, like variations in the Earths orbit, not all known periods have a known cause and need to be studied further.

VII. Figures

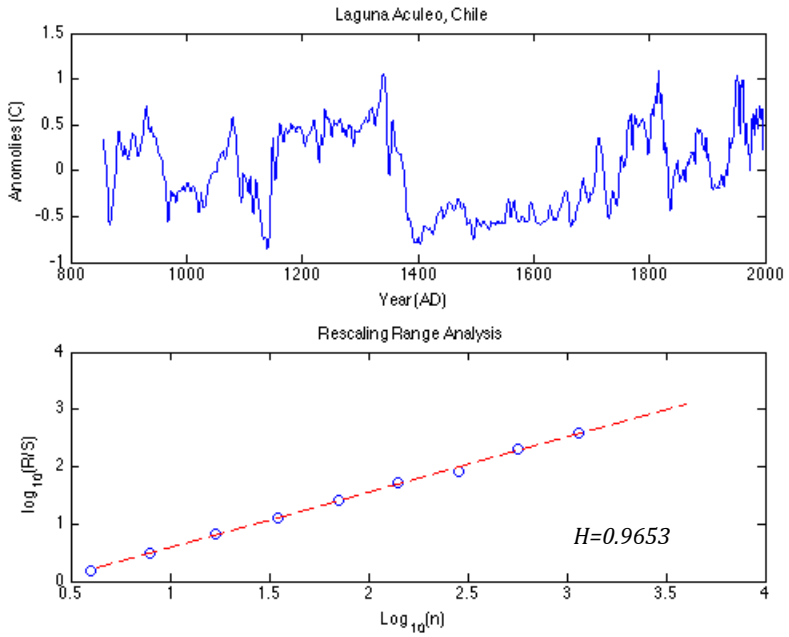

Fig. 1. Top panel: Laguna Aculeo, Chile proxy temperature record. Bottom panel: log(R/S) versus log(n) rescaling range analysis show temperature records is fractal.

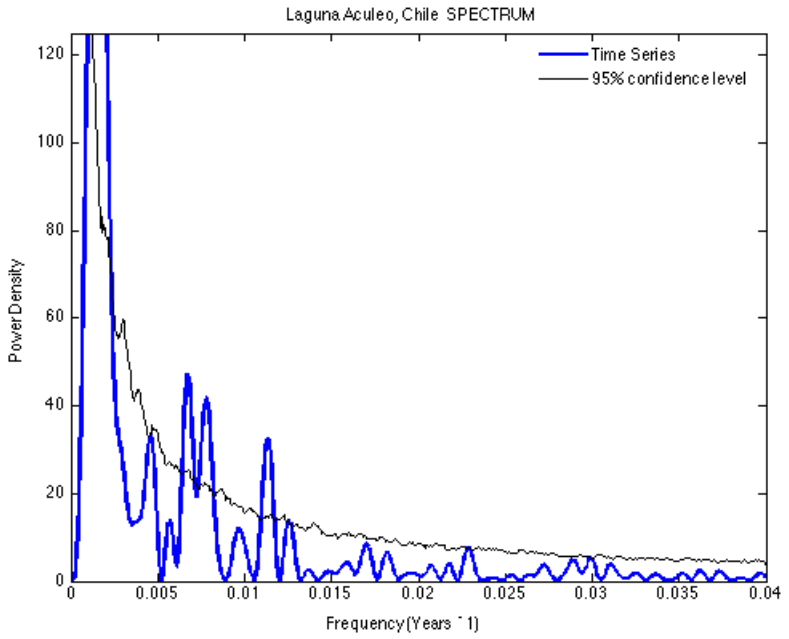

Fig. 2. Power spectrum analysis using DFT of Laguna Aculeo, Chile proxy temperature record (blue) with the 95% confidence level using 1000 Monte Carlo simulations (black).

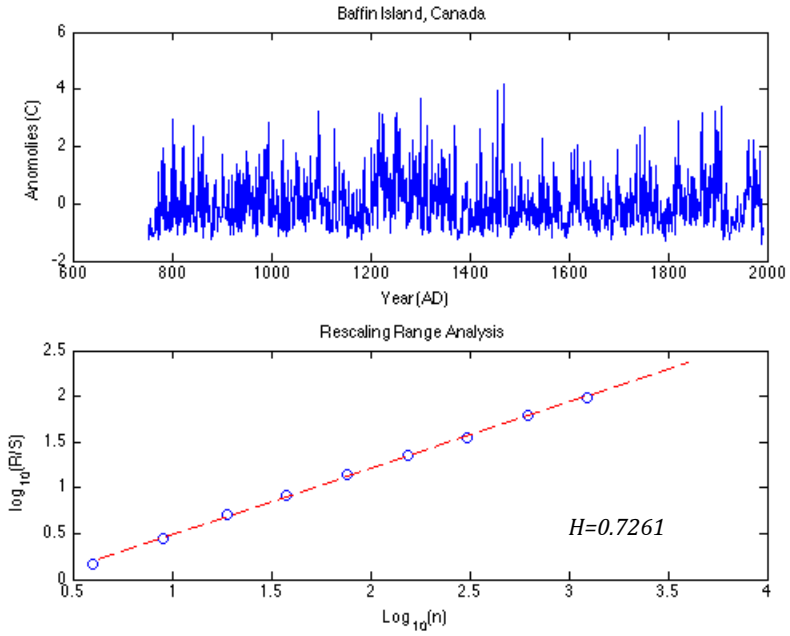

Fig. 3. Top panel: Baffin Island, Canada proxy temperature record. Bottom panel: log(R/S) versus log(n) rescaling range analysis show temperature records is fractal.

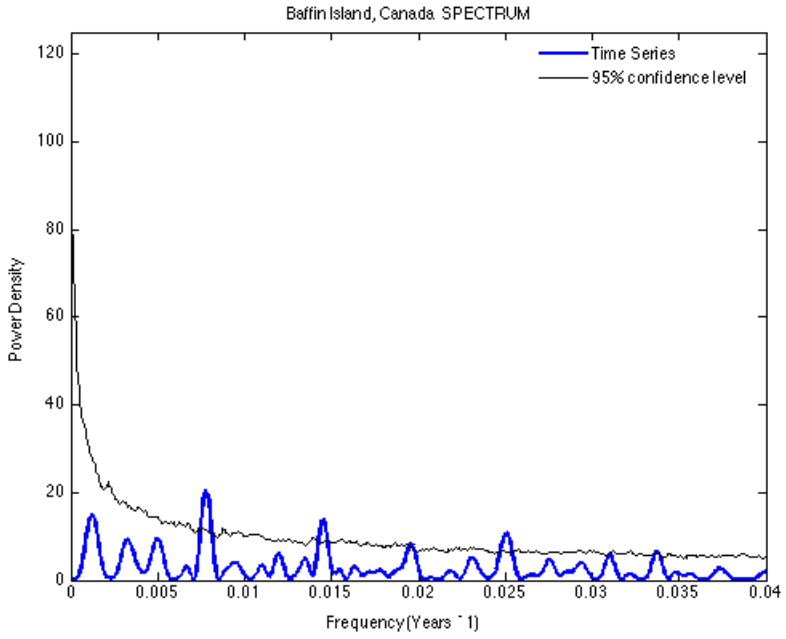

Fig. 4. Power spectrum analysis using DFT of Baffin Island, Canada proxy temperature record (blue) with the 95% confidence level using 1000 Monte Carlo simulations (black).

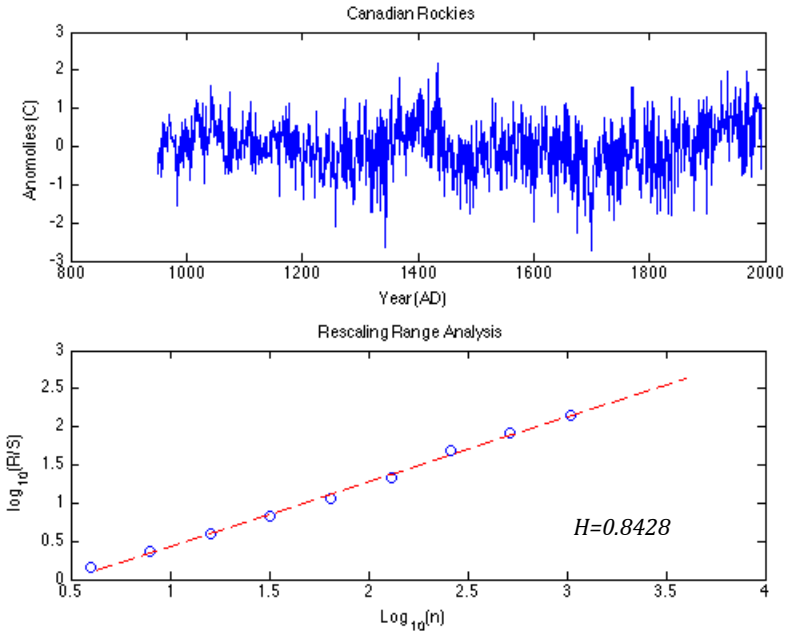

Fig. 5. Top panel: Canadian Rockies proxy temperature record. Bottom panel: log(R/S) versus log(n) rescaling range analysis show temperature records is fractal.

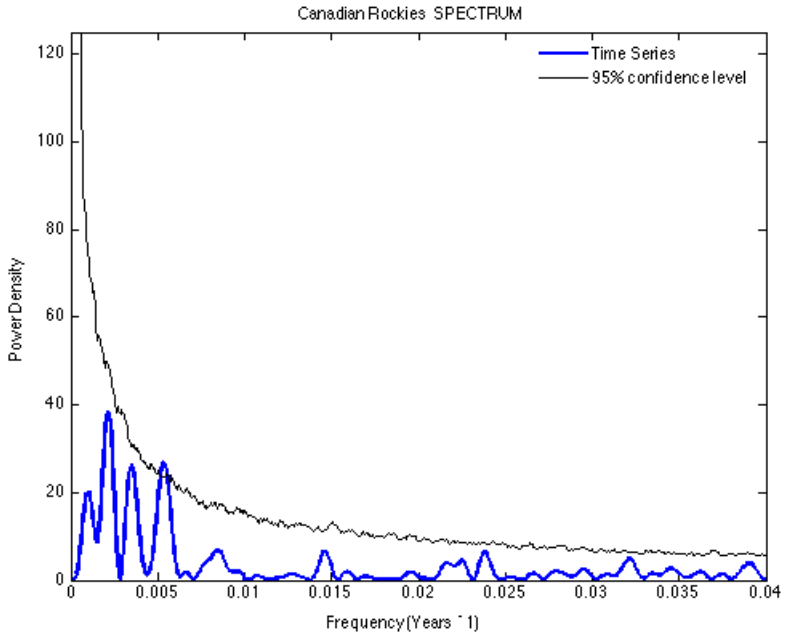

Fig. 6. Power spectrum analysis using DFT of Canadian Rockies proxy temperature record (blue) with the 95% confidence level using 1000 Monte Carlo simulations (black).

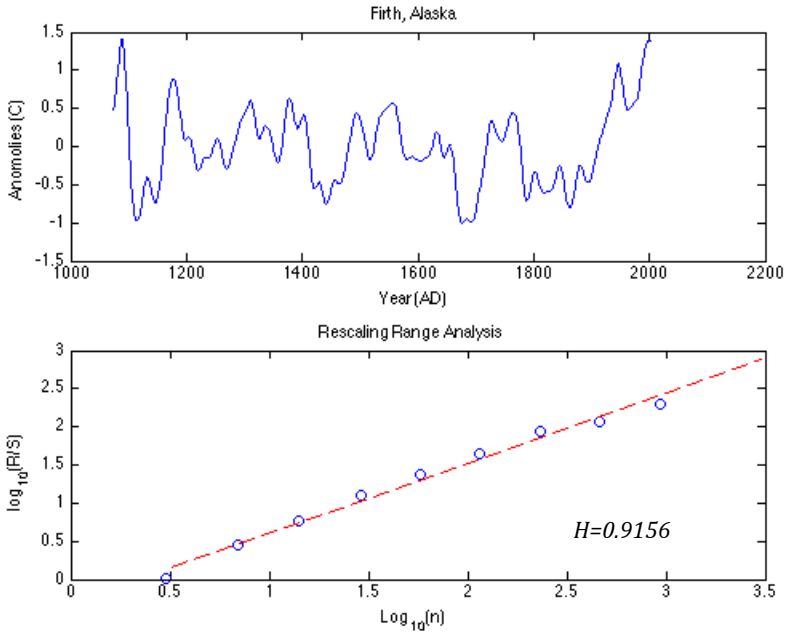

Fig. 7. Top panel: Firth, Alaska proxy temperature record. Bottom panel: log(R/S) versus log(n) rescaling range analysis show temperature records is fractal.

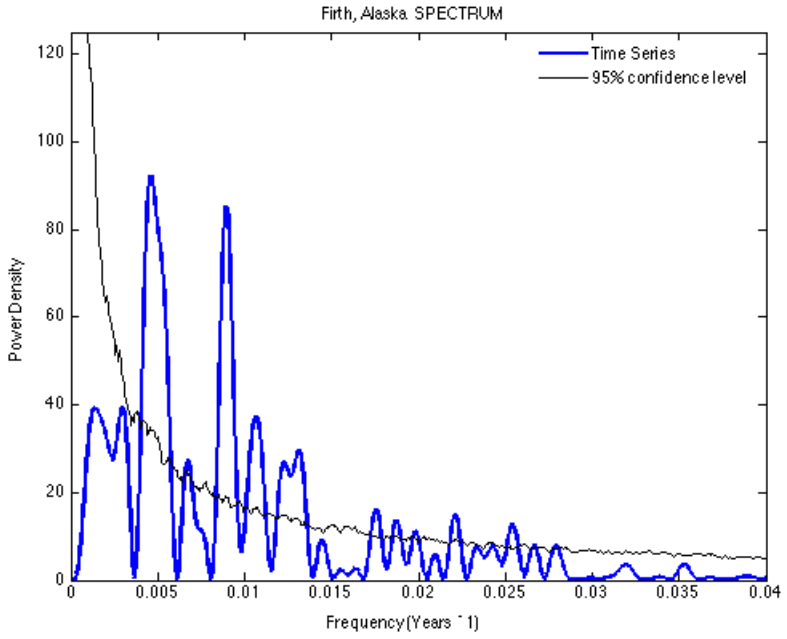

Fig. 8. Power spectrum analysis using DFT of Firth, Alaska proxy temperature record (blue) with the 95% confidence level using 1000 Monte Carlo simulations (black).

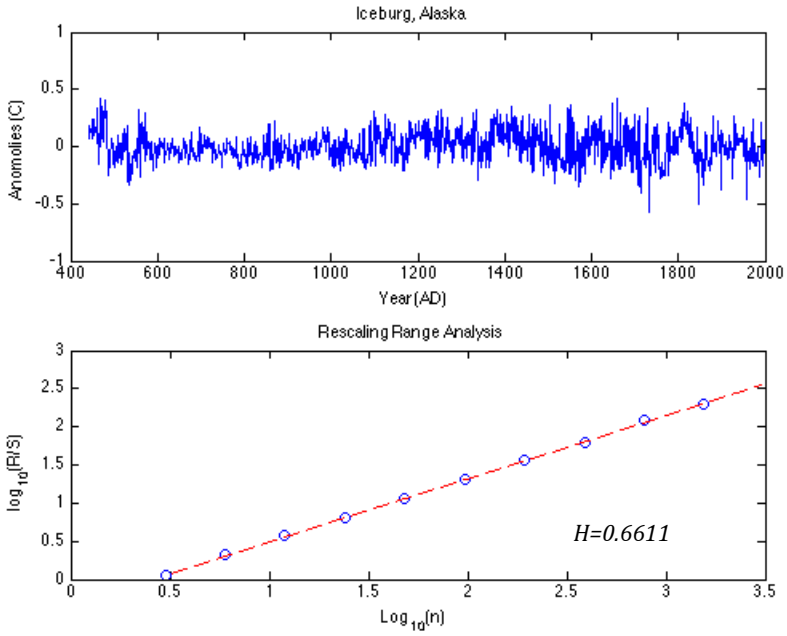

Fig. 9. Top panel: Iceberg, Alaska proxy temperature record. Bottom panel: log(R/S) versus log(n) rescaling range analysis show temperature records is fractal.

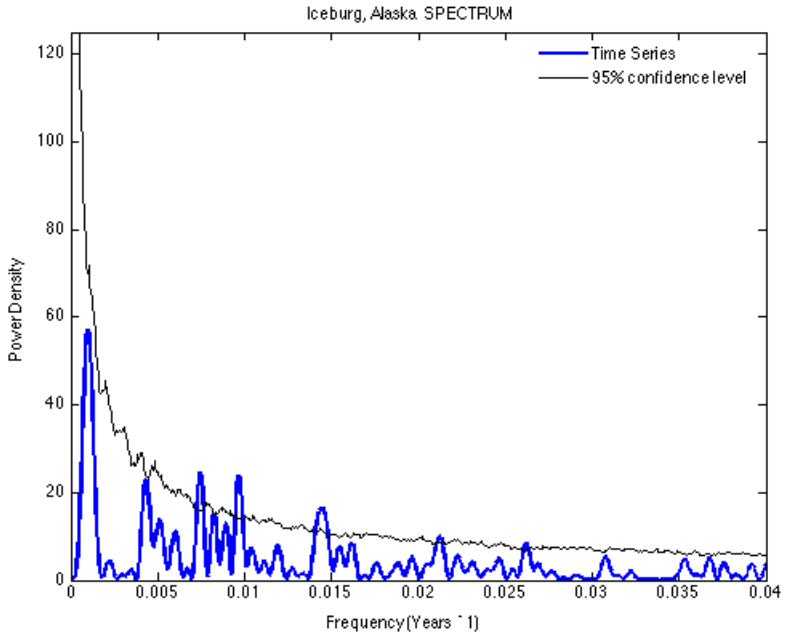

Fig. 10. Power spectrum analysis using DFT Iceberg, Alaska proxy temperature record (blue) with the 95% confidence level using 1000 Monte Carlo simulations (black).

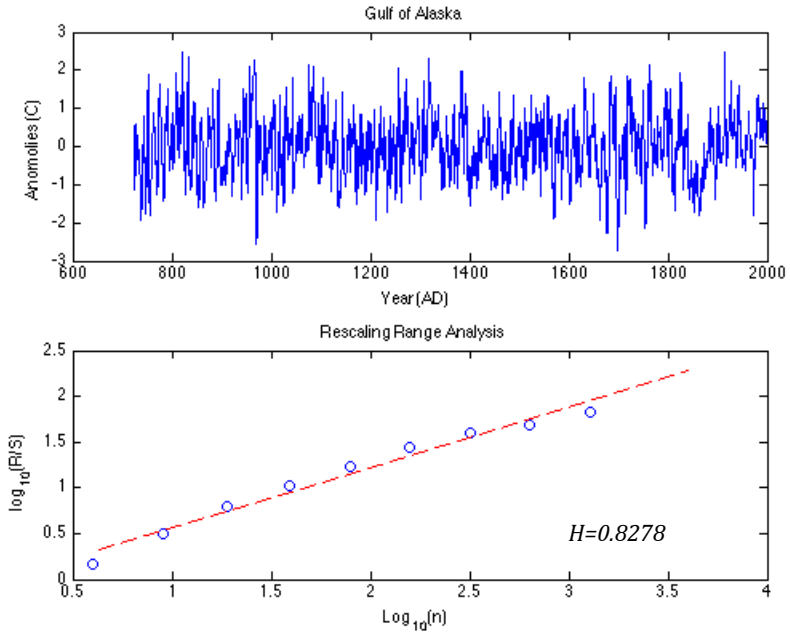

Fig. 11. Top panel: Gulf of Alaska, USA proxy temperature record. Bottom panel: log(R/S) versus log(n) rescaling range analysis show temperature records is fractal.

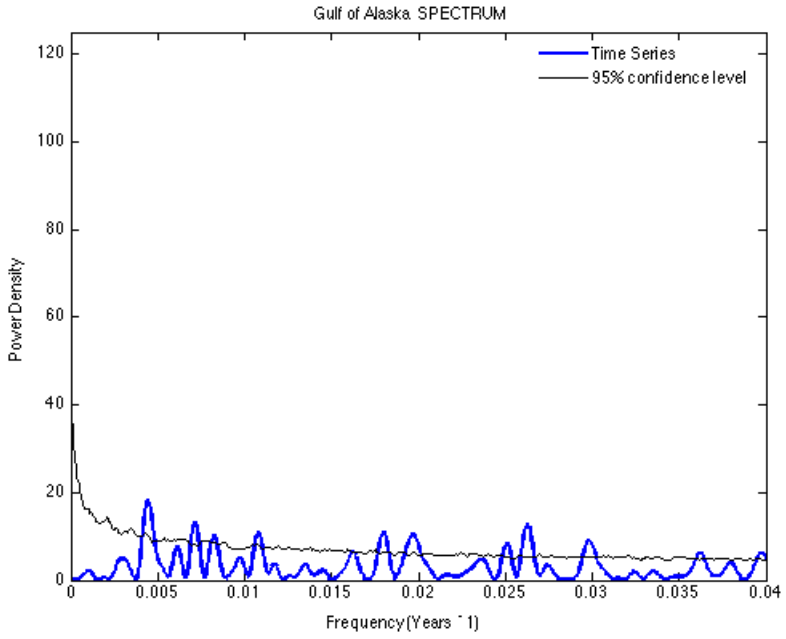

Fig. 12. Power spectrum analysis using DFT Gulf of Alaska, USA proxy temperature record (blue) with the 95% confidence level using 1000 Monte Carlo simulations (black).

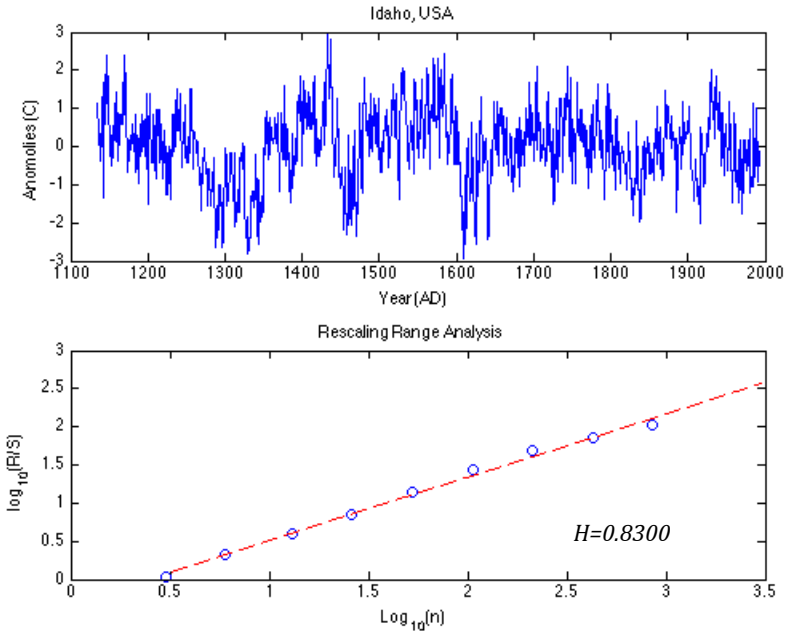

Fig. 13. Top panel: Idaho, USA proxy temperature record. Bottom panel: log(R/S) versus log(n) rescaling range analysis show temperature records is fractal.

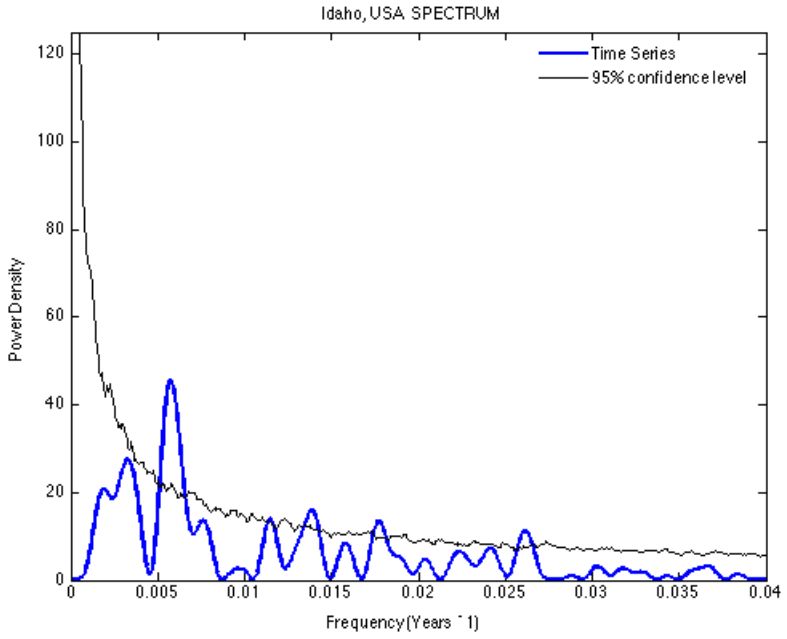

Fig. 14. Power spectrum analysis using DFT of Idaho, USA proxy temperature record (blue) with the 95% confidence level using 1000 Monte Carlo simulations (black).

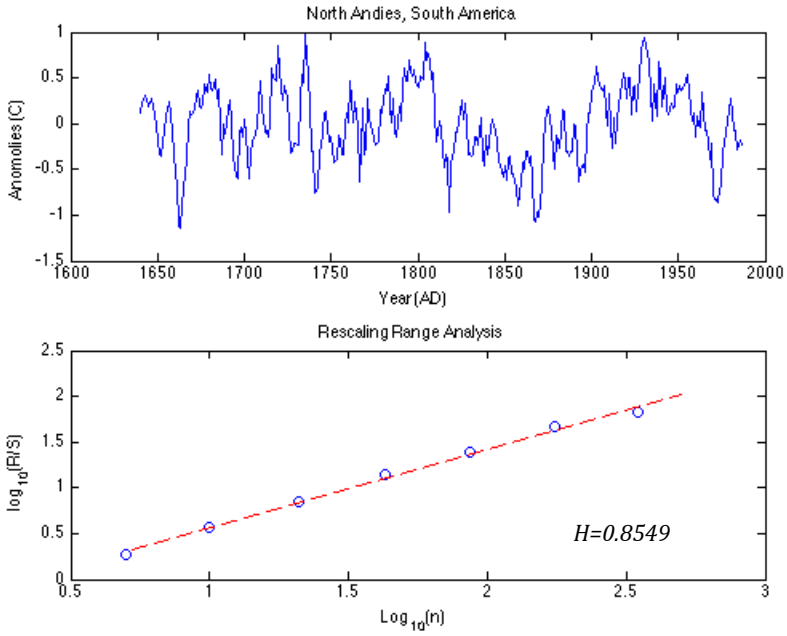

Fig. 15. Top panel: Northern Andes, South America proxy temperature record. Bottom panel: log(R/S) versus log(n) rescaling range analysis show temperature records is fractal.

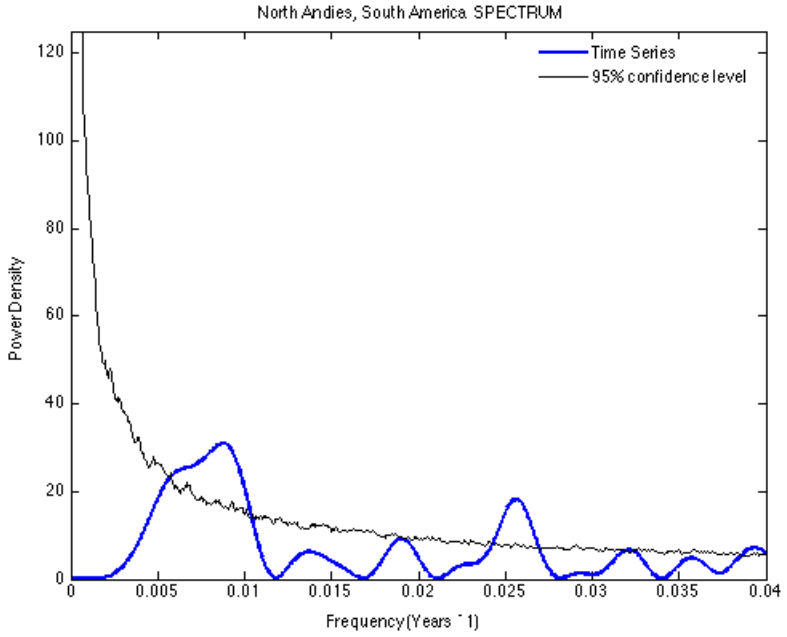

F**ig. 16.** Power spectrum analysis using DFT of Northern Andes, South America proxy temperature record (blue) with the 95% confidence level using 1000 Monte Carlo simulations (black).

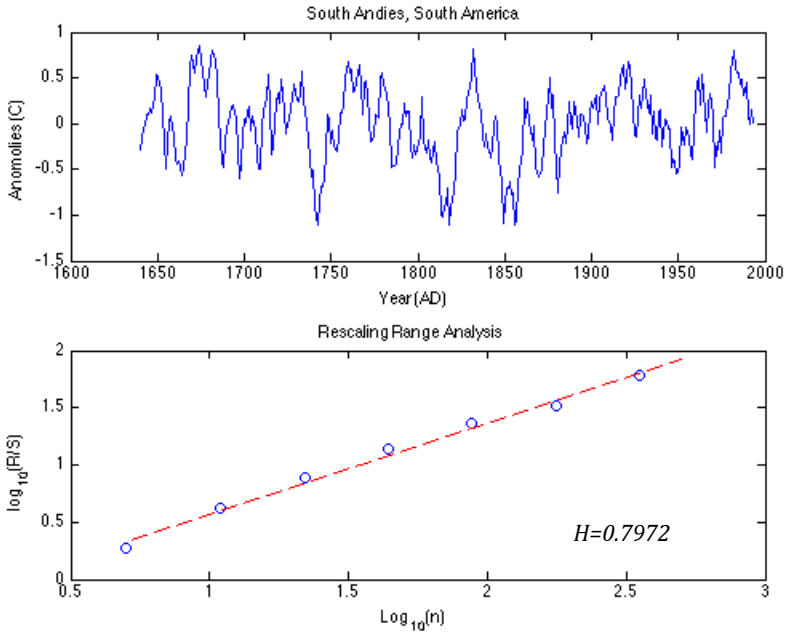

Fig. 17. Top panel: Southern Andes, South America proxy temperature record. Bottom panel: log(R/S) versus log(n) rescaling range analysis show temperature records is fractal.

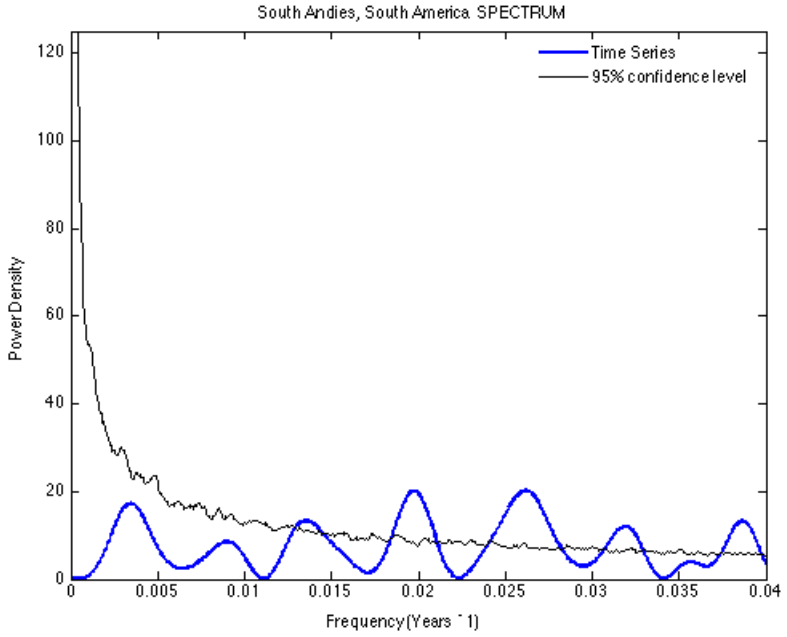

Fig. 18. Power spectrum analysis using DFT of Southern Andes, South America proxy temperature record (blue) with the 95% confidence level using 1000 Monte Carlo simulations (black).

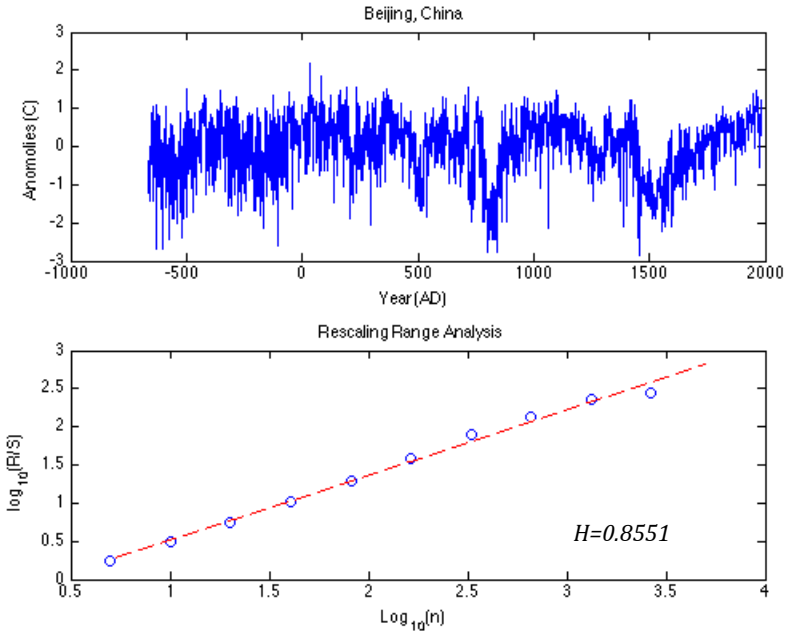

Fig. 19. Top panel: Beijing, China proxy temperature record. Bottom panel: log(R/S) versus log(n) rescaling range analysis show temperature records is fractal.

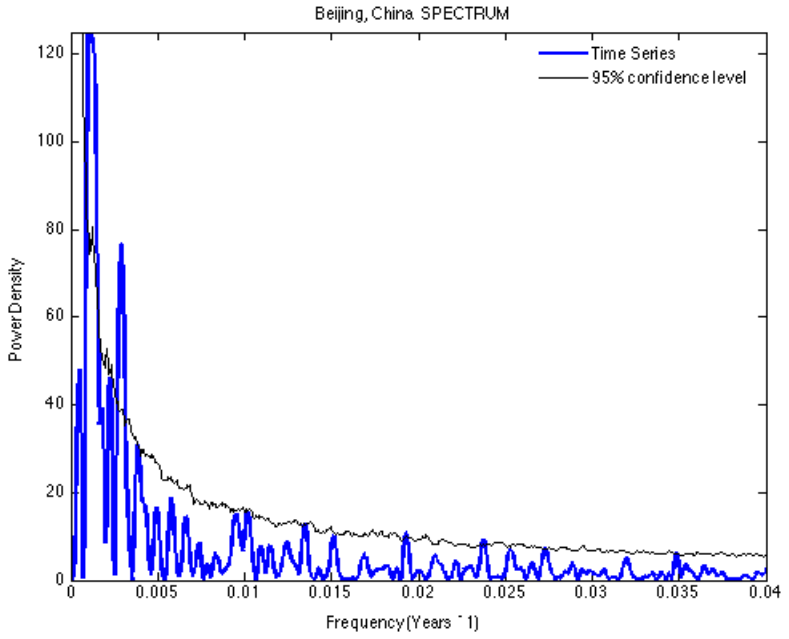

Fig. 20. Power spectrum analysis using DFT of Beijing, China proxy temperature record (blue) with the 95% confidence level using 1000 Monte Carlo simulations (black).

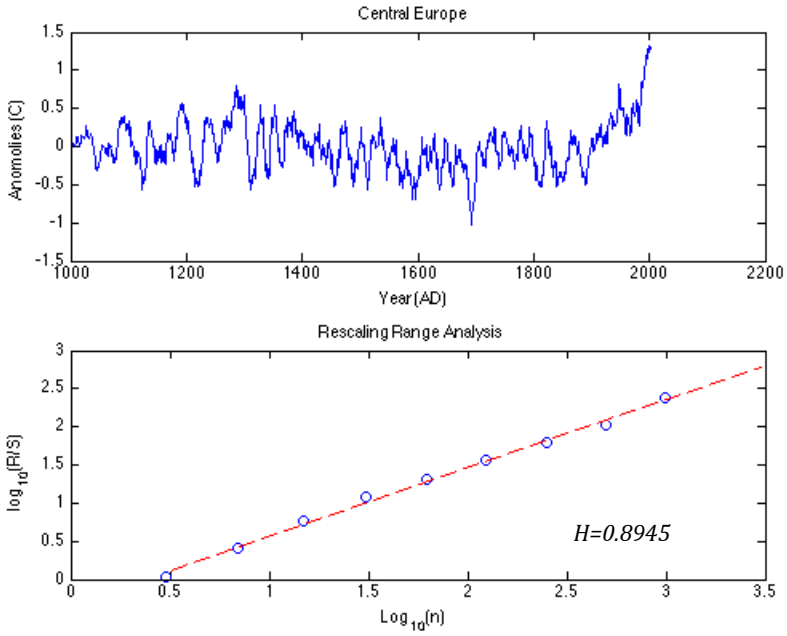

Fig. 21. Top panel: Central Europe proxy temperature record. Bottom panel: log(R/S) versus log(n) rescaling range analysis show temperature records is fractal.

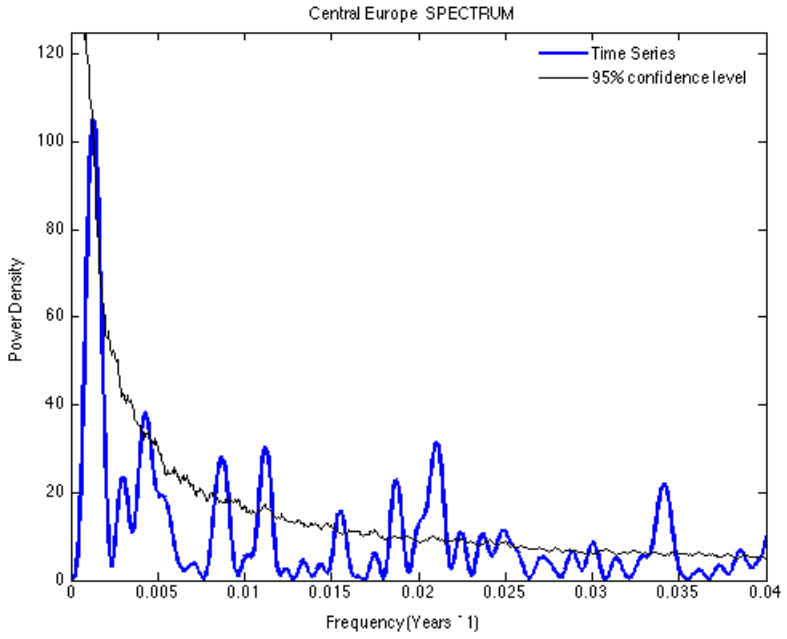

Fig. 22. Power spectrum analysis using DFT of Central Europe proxy temperature record (blue) with the 95% confidence level using 1000 Monte Carlo simulations (black).

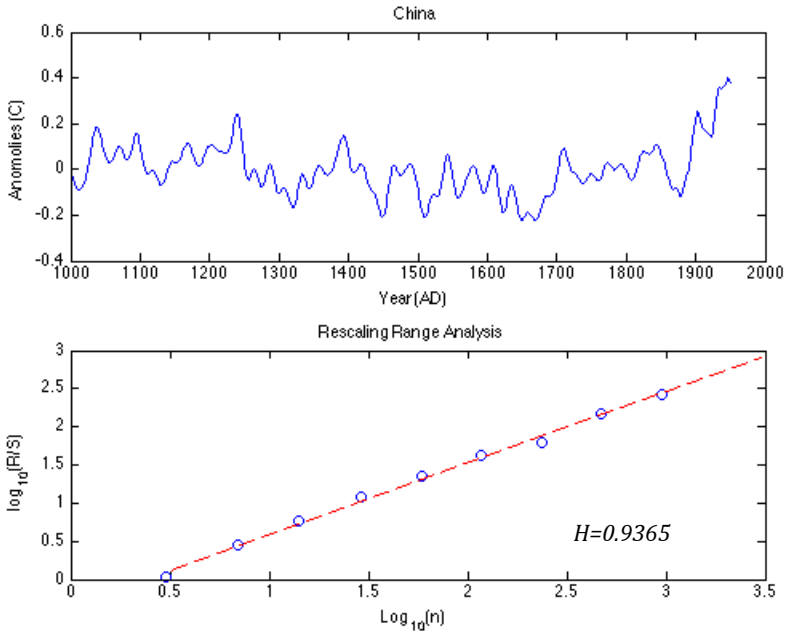

Fig. 23. Top panel: China proxy temperature record. Bottom panel: log(R/S) versus log(n) rescaling range analysis show temperature records is fractal.

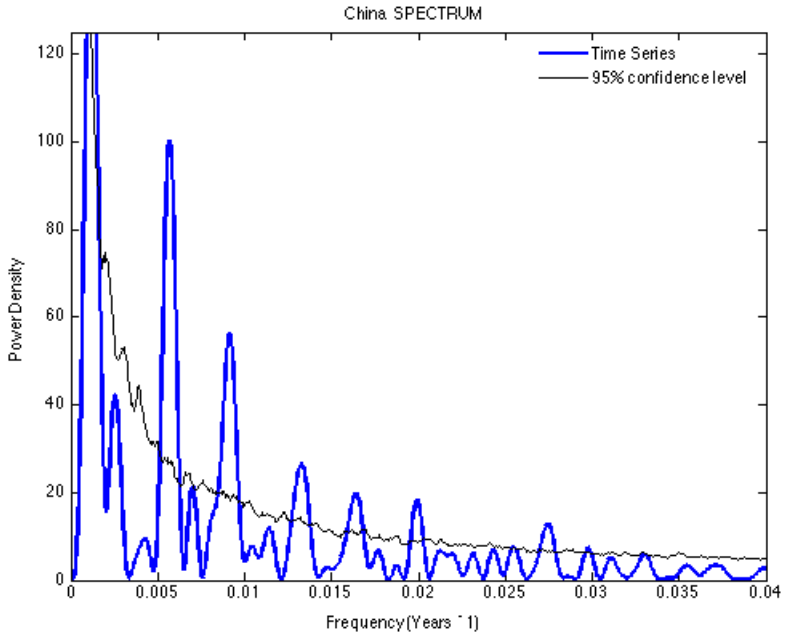

Fig. 24. Power spectrum analysis using DFT China proxy temperature record (blue) with the 95% confidence level using 1000 Monte Carlo simulations (black).

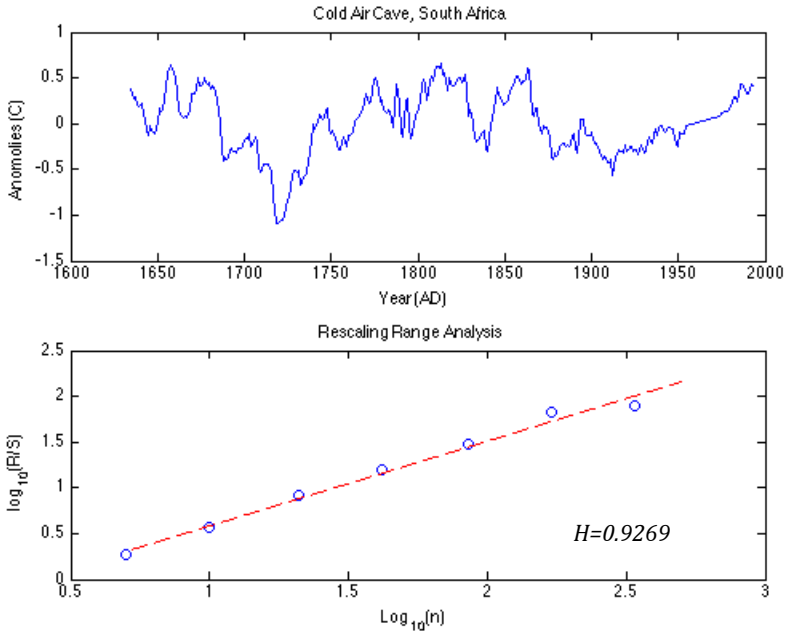

Fig. 25. Top panel: Cold Air Cave, South Africa proxy temperature record. Bottom panel: log(R/S) versus log(n) rescaling range analysis show temperature records is fractal.

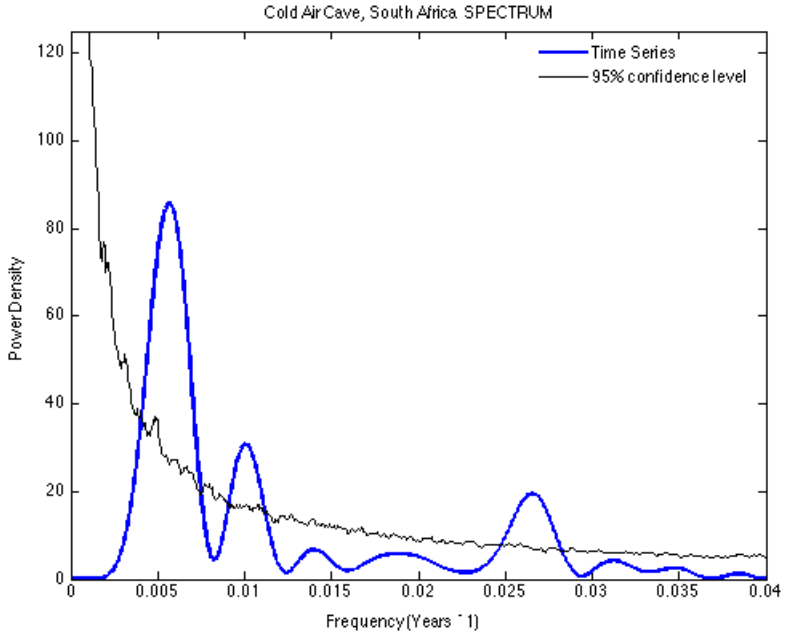

Fig. 26. Power spectrum analysis using DFT of Cold Air Cave, South Africa proxy temperature record (blue) with the 95% confidence level using 1000 Monte Carlo simulations (black).

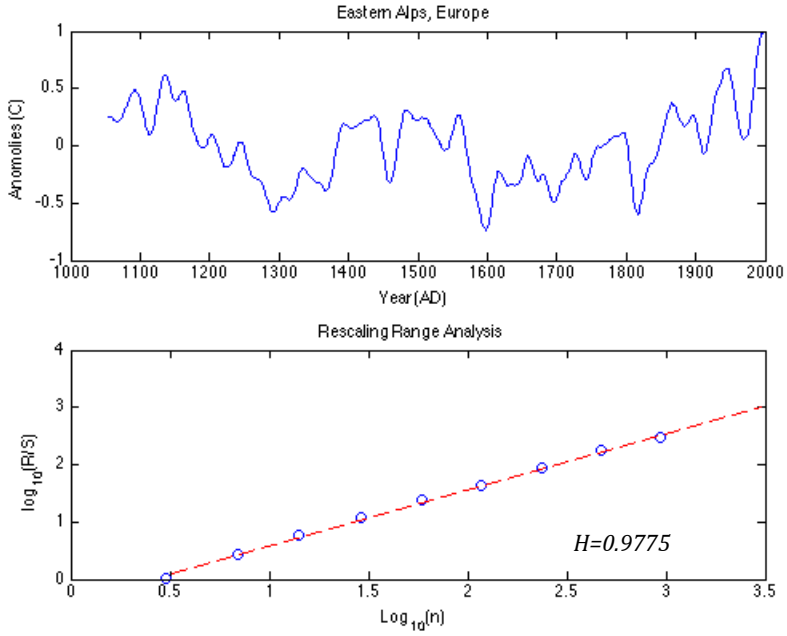

Fig. 27. Top panel: Eastern Alps, Europe proxy temperature record. Bottom panel: log(R/S) versus log(n) rescaling range analysis show temperature records is fractal.

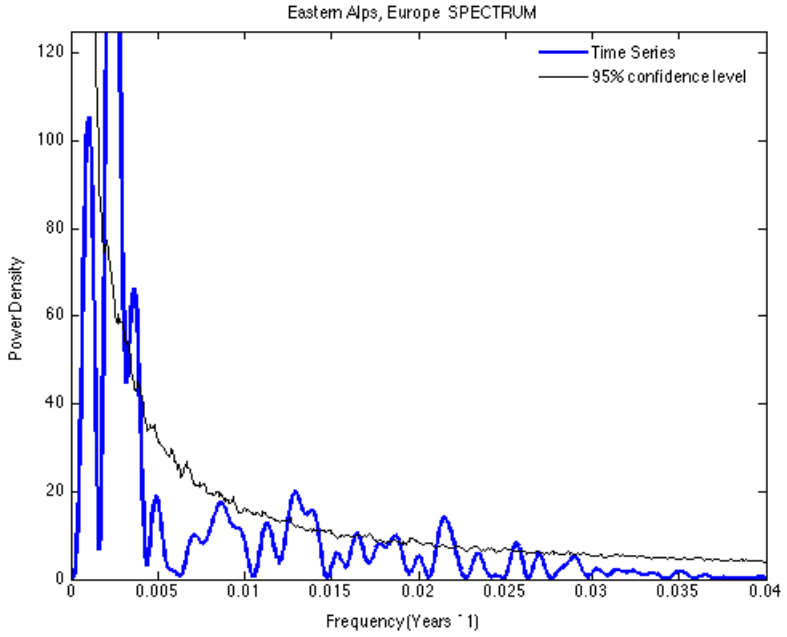

Fig. 28. Power spectrum analysis using DFT of Eastern Alps, Europe proxy temperature record (blue) with the 95% confidence level using 1000 Monte Carlo simulations (black).

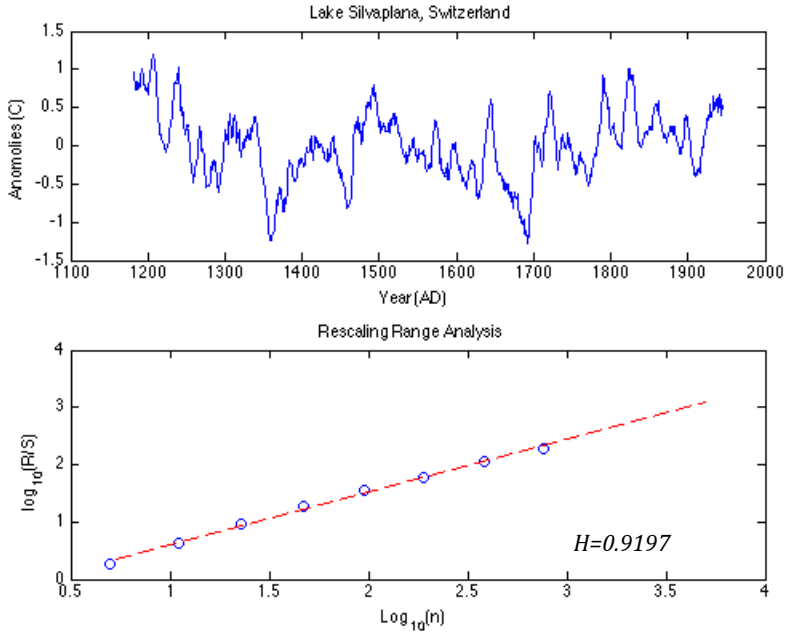

Fig. 29. Top panel: Lake Silvaplana, Switzerland proxy temperature record. Bottom panel: log(R/S) versus log(n) rescaling range analysis show temperature records is fractal.

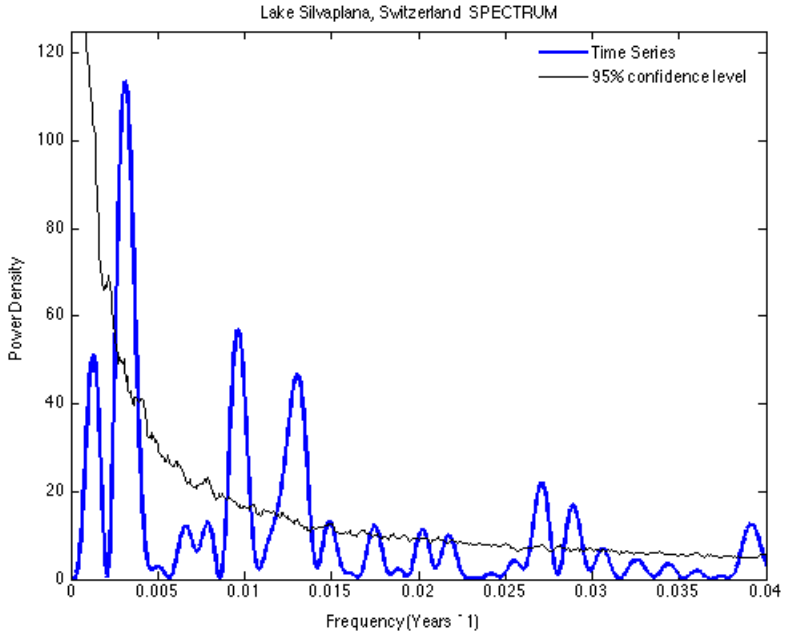

F**ig. 30.** Power spectrum analysis using DFT of Lake Silvaplana, Switzerland proxy temperature record (blue) with the 95% confidence level using 1000 Monte Carlo simulations (black).

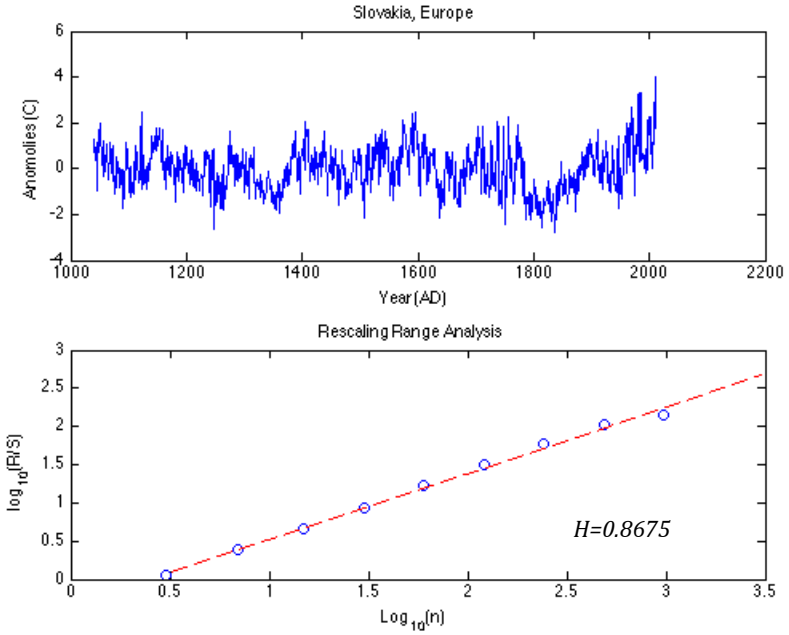

Fig. 31. Top panel: Slovakia, Europe proxy temperature record. Bottom panel: log(R/S) versus log(n) rescaling range analysis show temperature records is fractal.

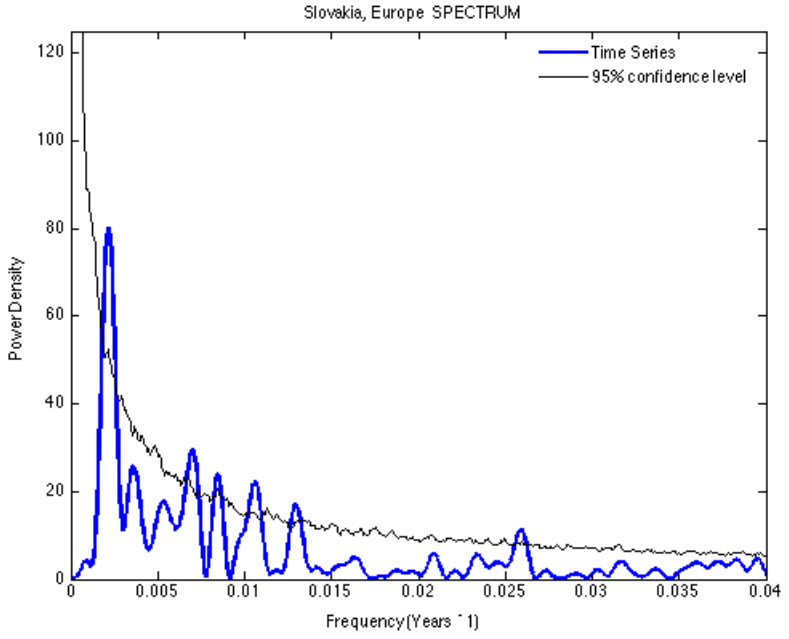

Fig. 32. Power spectrum analysis using DFT of Slovakia, Europe proxy temperature record (blue) with the 95% confidence level using 1000 Monte Carlo simulations (black).

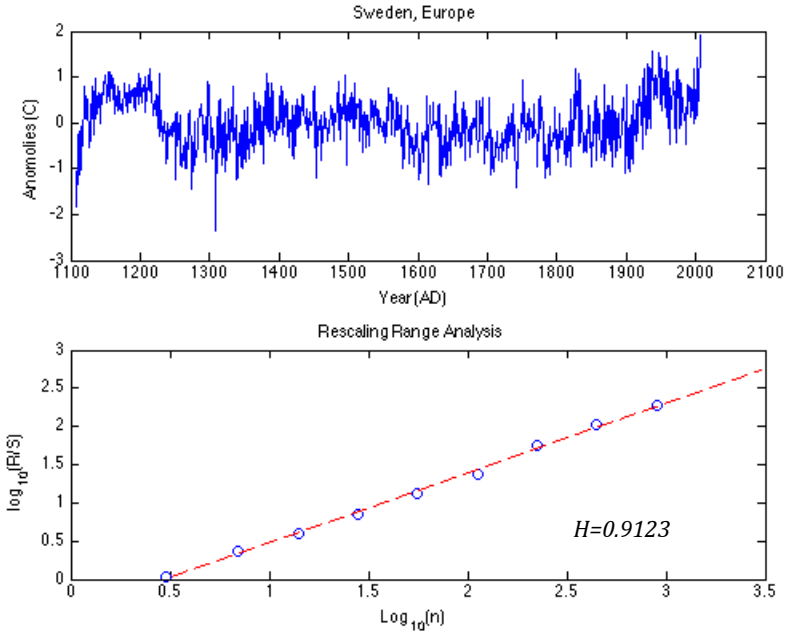

Fig. 33. Top panel: Sweden, Europe proxy temperature record. Bottom panel: log(R/S) versus log(n) rescaling range analysis show temperature records is fractal.

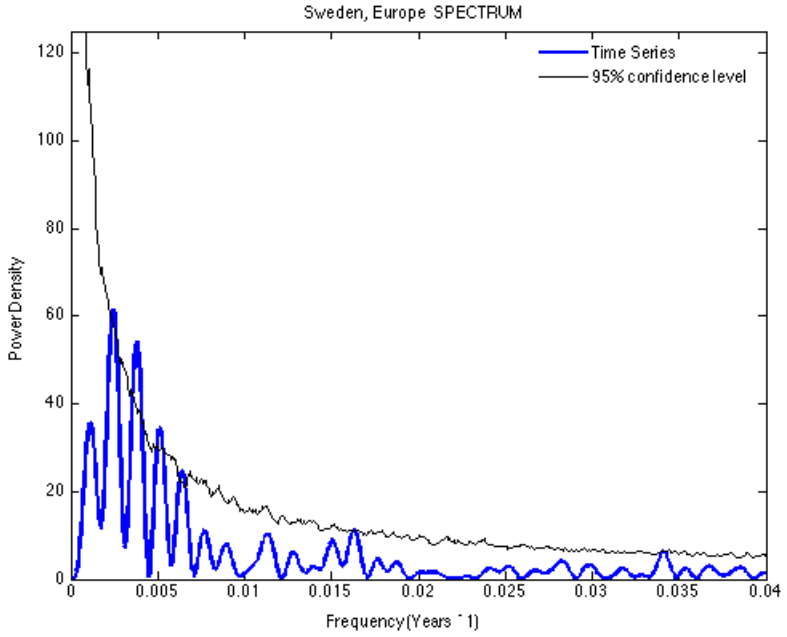

Fig. 34. Power spectrum analysis using DFT of Sweden, Europe proxy temperature record (blue) with the 95% confidence level using 1000 Monte Carlo simulations (black).

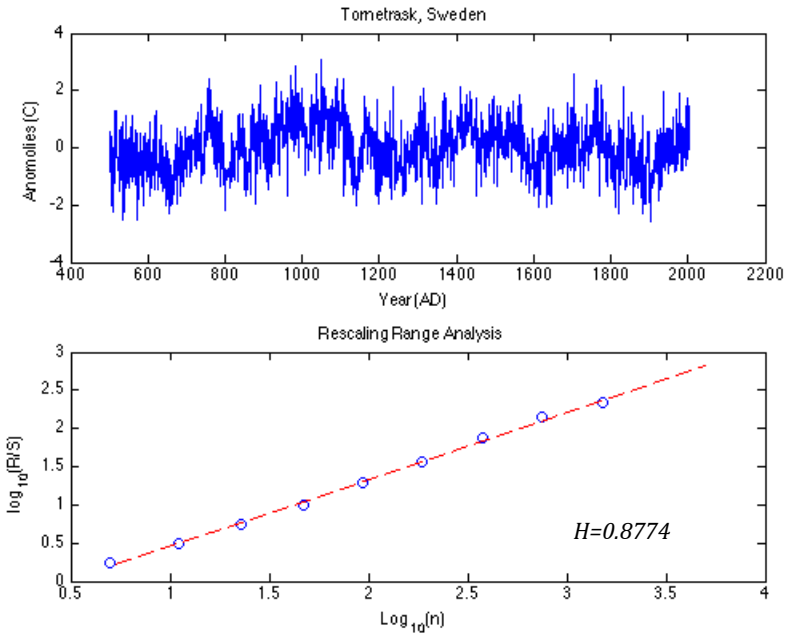

Fig. 35. Top panel: Tornetrask, Sweden proxy temperature record. Bottom panel: log(R/S) versus log(n) rescaling range analysis show temperature records is fractal.

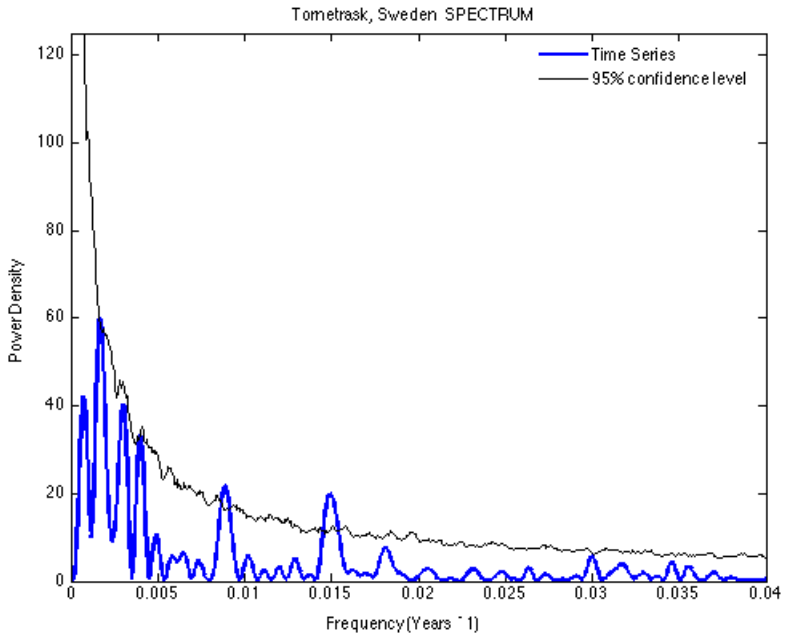

Fig. 36. Power spectrum analysis using DFT of Tornetrask, Sweden proxy temperature record (blue) with the 95% confidence level using 1000 Monte Carlo simulations (black).

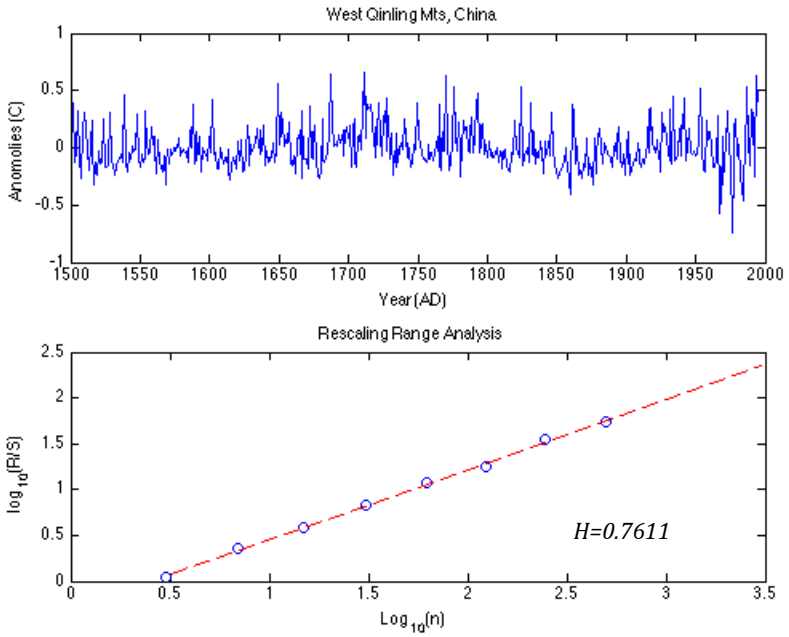

Fig. 37. Top panel: West Qinling Mts, China proxy temperature record. Bottom panel: log(R/S) versus log(n) rescaling range analysis show temperature records is fractal.

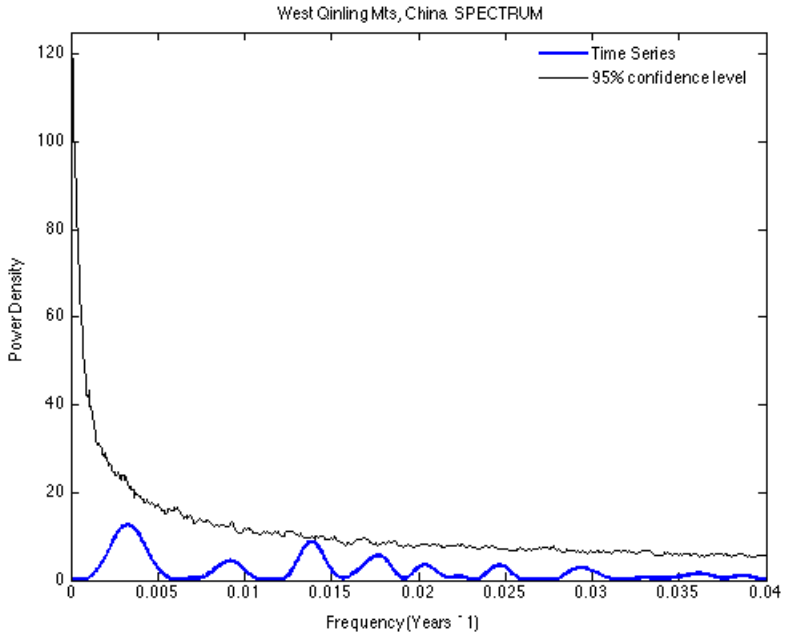

Fig. 38. Power spectrum analysis using DFT of West Qinling Mts, China proxy temperature record (blue) with the 95% confidence level using 1000 Monte Carlo simulations (black).

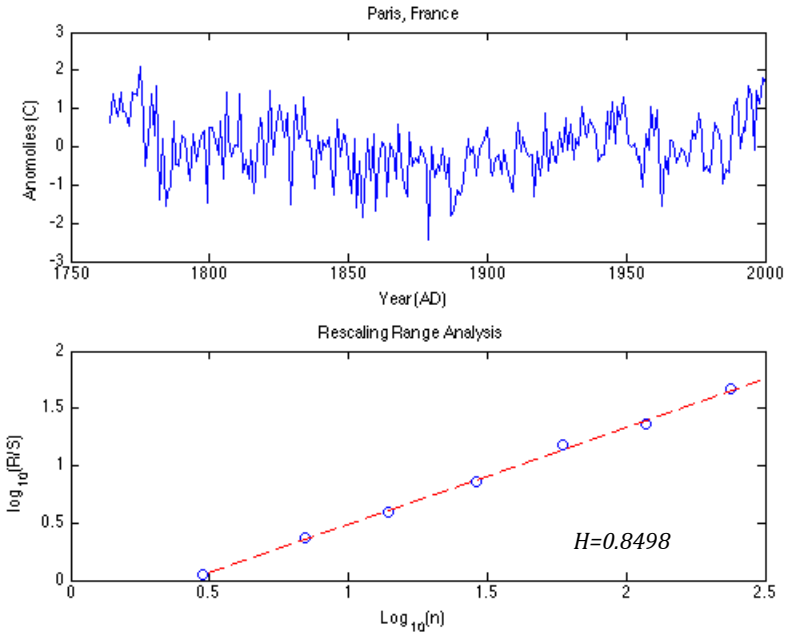

Fig. 39. Top panel: Paris, France instrumental temperature record. Bottom panel: log(R/S) versus log(n) rescaling range analysis show temperature records is fractal.

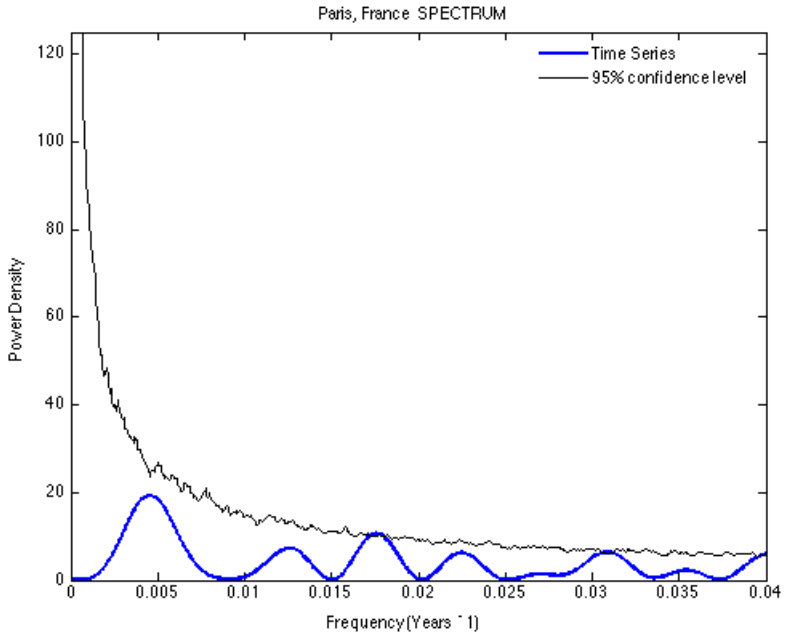

Fig. 40. Power spectrum analysis using DFT of Paris, France instrumental temperature record (blue) with the 95% confidence level using 1000 Monte Carlo simulations (black).

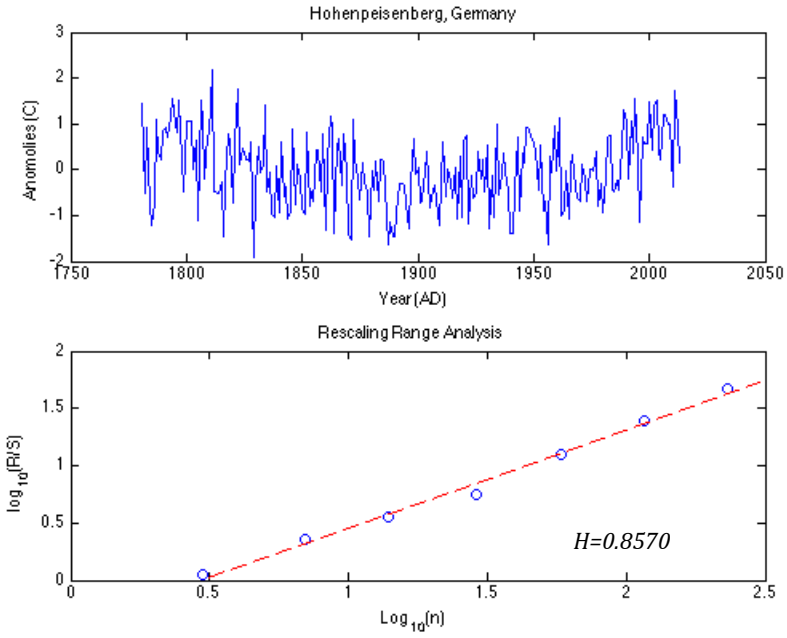

Fig. 41. Top panel: Hohenpeisenberg, Germany instrumental temperature record. Bottom panel: log(R/S) versus log(n) rescaling range analysis show temperature records is fractal.

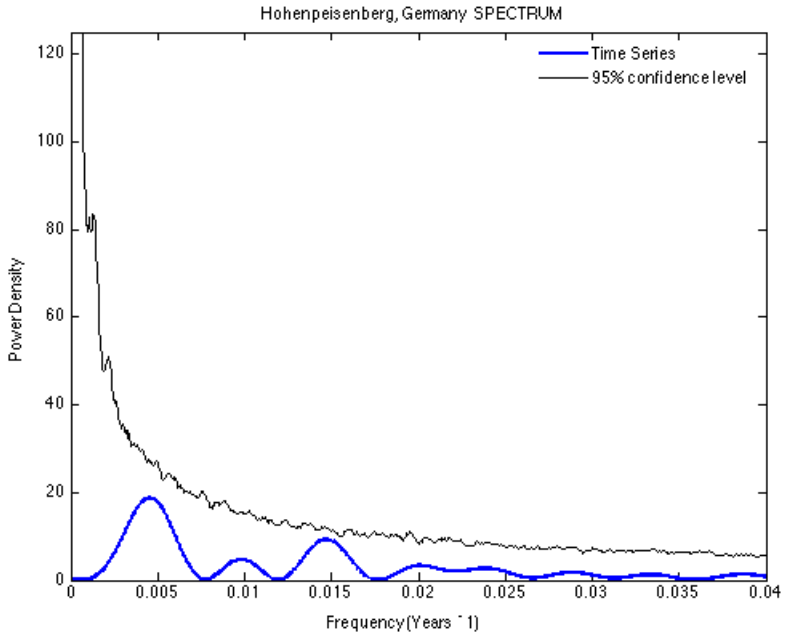

Fig. 42. Power spectrum analysis using DFT of Hohenpeisenberg, Germany instrumental temperature record (blue) with the 95% confidence level using 1000 Monte Carlo simulations (black).

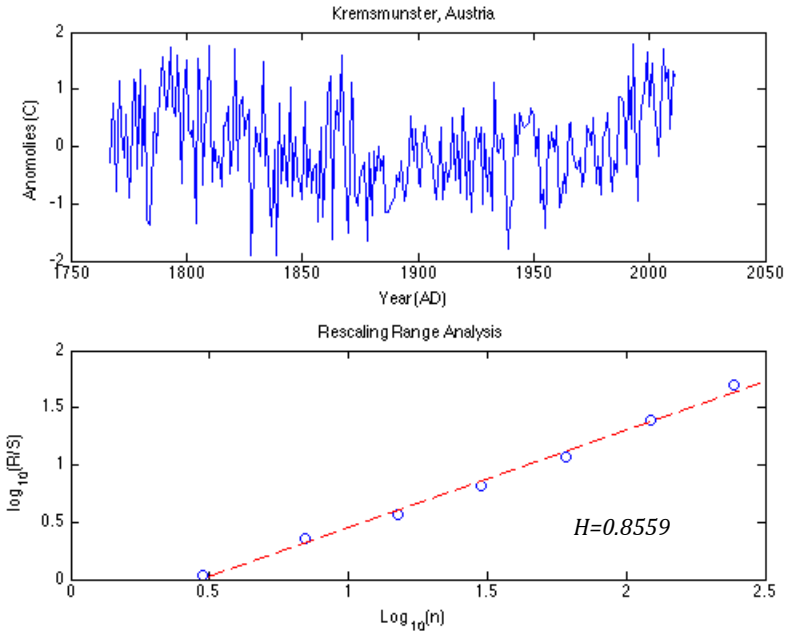

Fig. 43. Top panel: Kremamunster, Austria instrumental temperature record. Bottom panel: log(R/S) versus log(n) rescaling range analysis show temperature records is fractal.

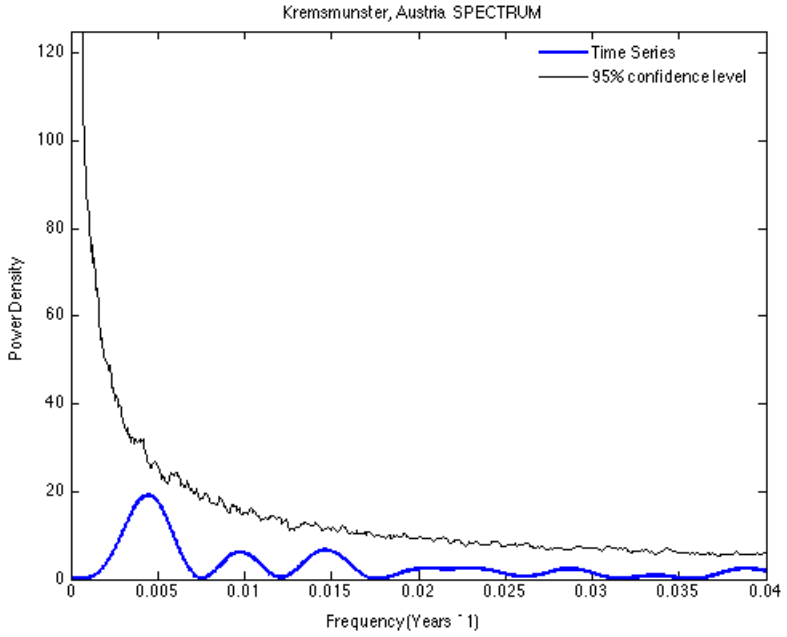

Fig. 44. Power spectrum analysis using DFT of Kremamunster, Austria instrumental proxy temperature record (blue) with the 95% confidence level using 1000 Monte Carlo simulations (black).

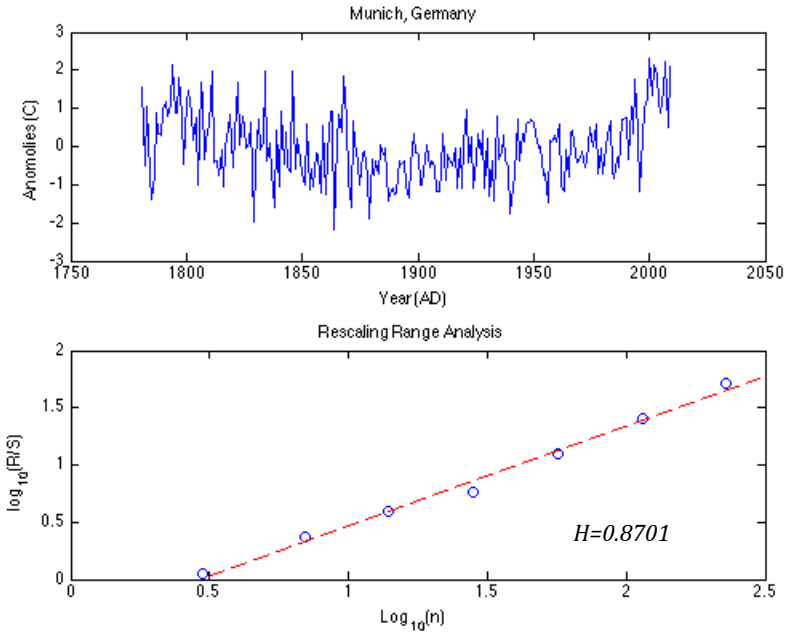

Fig. 45. Top panel: Munich, Germany instrumental temperature record. Bottom panel: log(R/S) versus log(n) rescaling range analysis show temperature records is fractal.

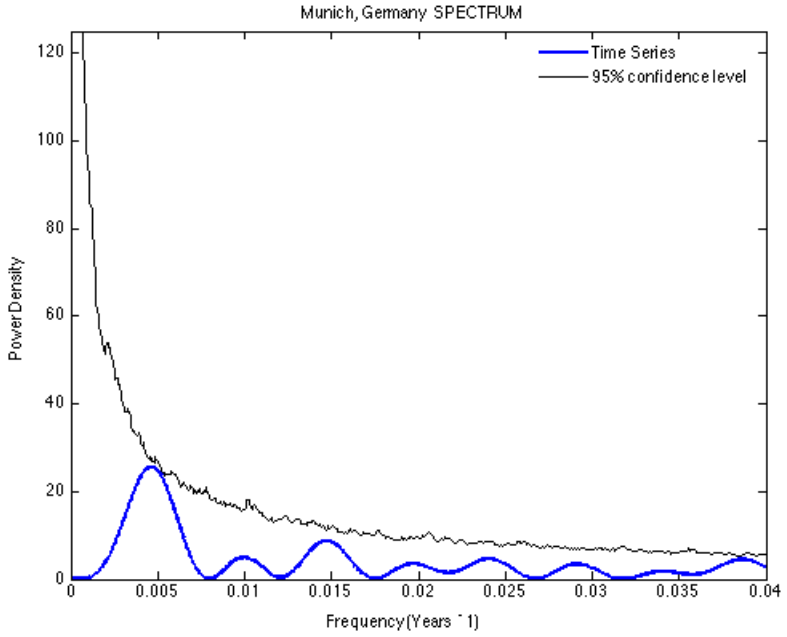

Fig. 46. Power spectrum analysis using DFT of Munich, Germany instrumental temperature record (blue) with the 95% confidence level using 1000 Monte Carlo simulations (black).

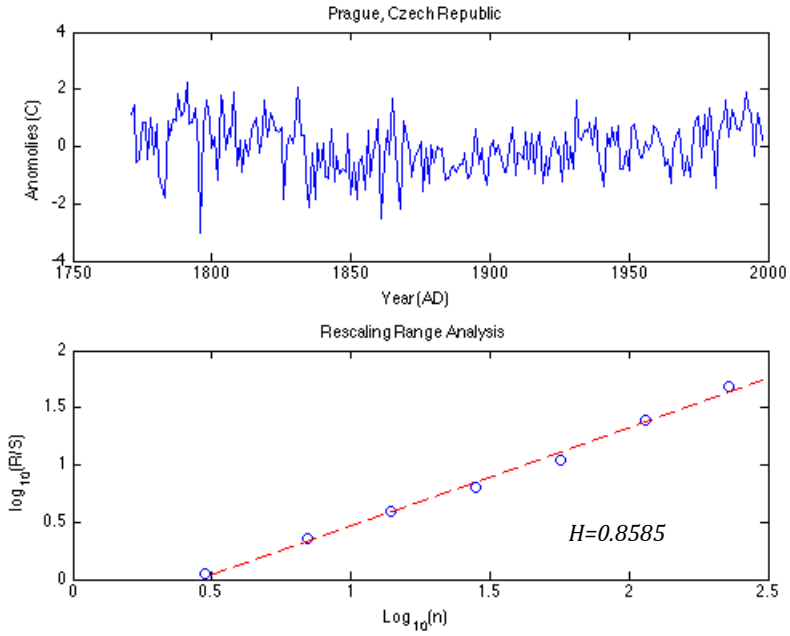

Fig. 47. Top panel: Prague, Austria instrumental temperature record. Bottom panel: log(R/S) versus log(n) rescaling range analysis show temperature records is fractal.

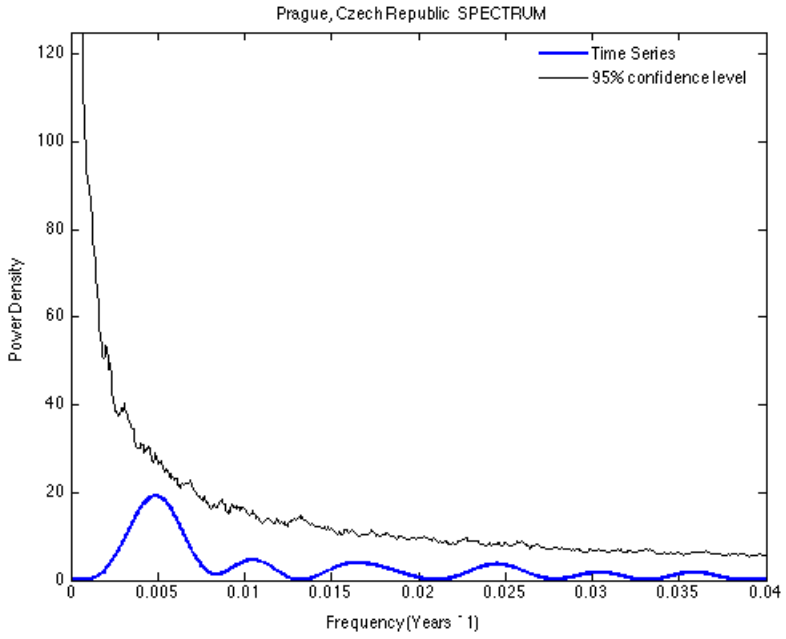

Fig. 48. Power spectrum analysis using DFT of Prague, Austria instrumental temperature record (blue) with the 95% confidence level using 1000 Monte Carlo simulations (black).

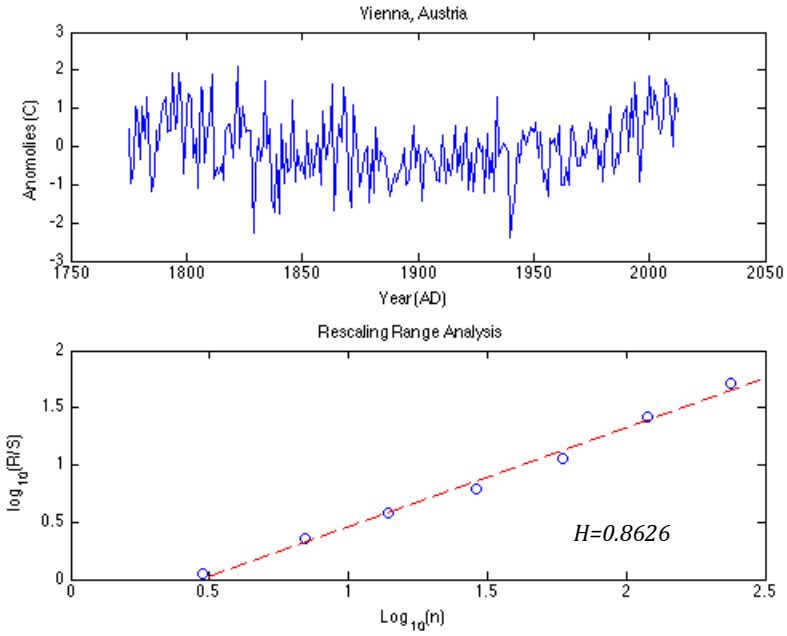

Fig. 49. Top panel Vienna, Austria instrumental temperature record. Bottom panel: log(R/S) versus log(n) rescaling range analysis show temperature records is fractal.

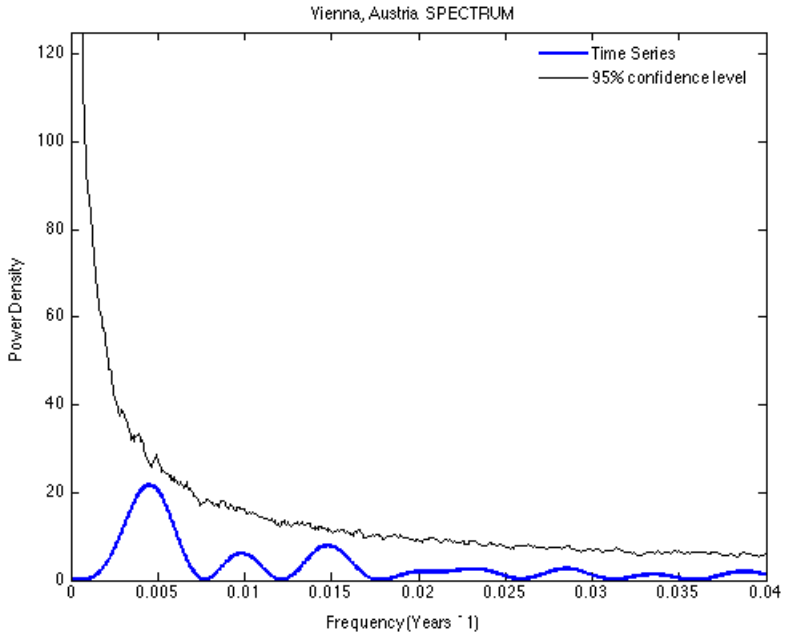

Fig. 50. Power spectrum analysis using DFT of Vienna, Austria instrumental temperature record (blue) with the 95% confidence level using 1000 Monte Carlo simulations (black).

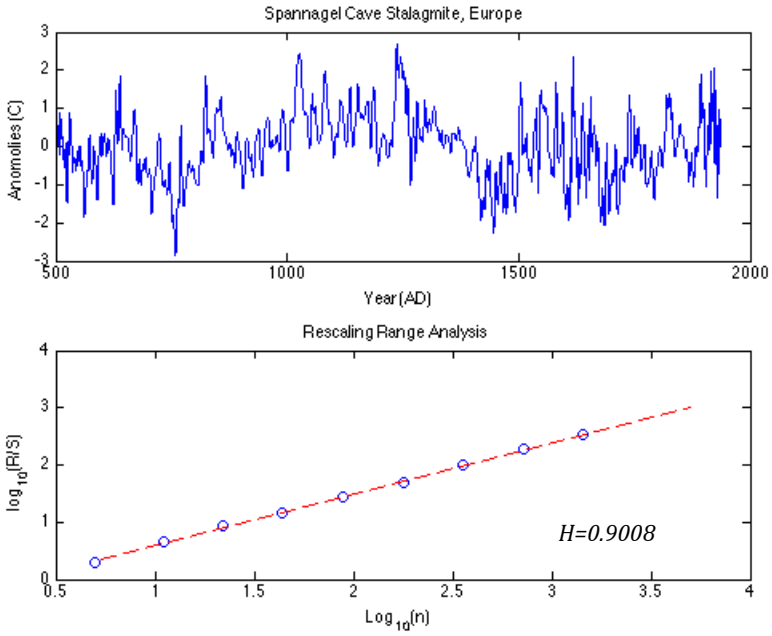

Fig. 51. Top panel: Spannagel Cave, Europe proxy temperature record. Bottom panel: log(R/S) versus log(n) rescaling range analysis show temperature records is fractal.

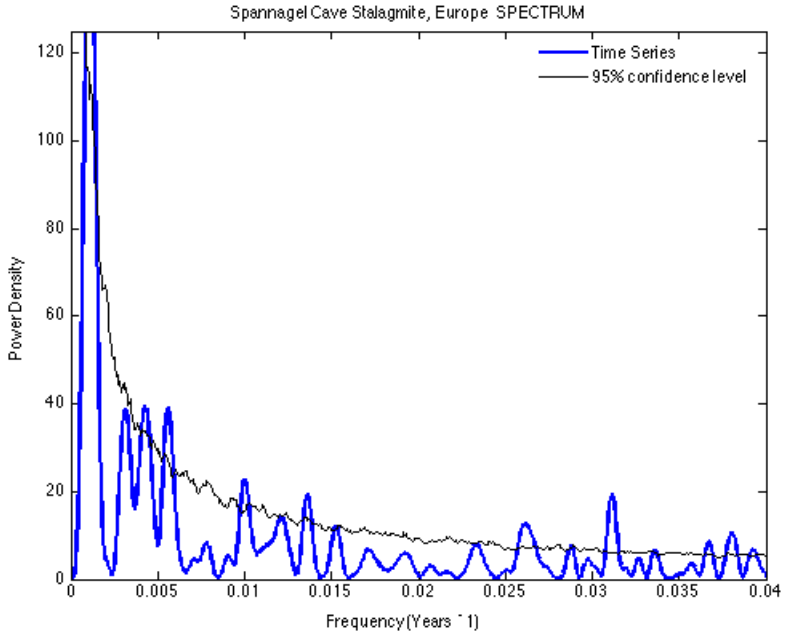

Fig. 52. Power spectrum analysis using DFT of Spannagel Cave, Europe proxy temperature record (blue) with the 95% confidence level using 1000 Monte Carlo simulations (black).

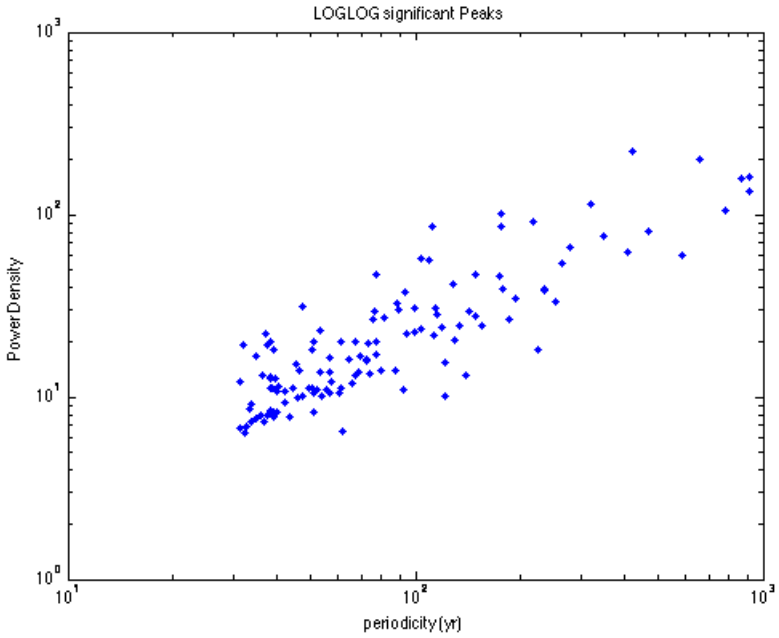

Fig. 53. Log-log plot of periods versus power of all significant peaks from all short-length temperature records. The line-of-best-fit with slope of $M = 0.18912$.

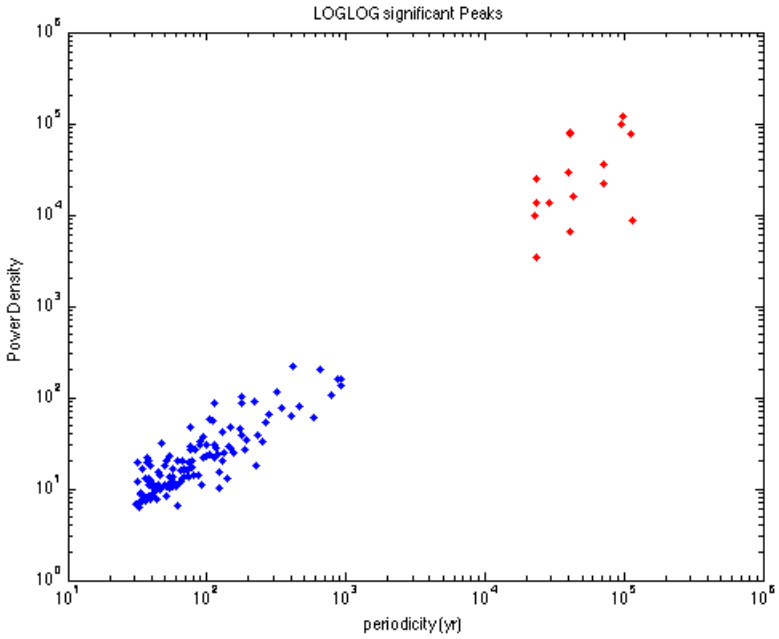

Fig. 54. Log-log plot of periods versus power of all significant peaks from all short-length temperature records (blue) and long-length temperature records (red).

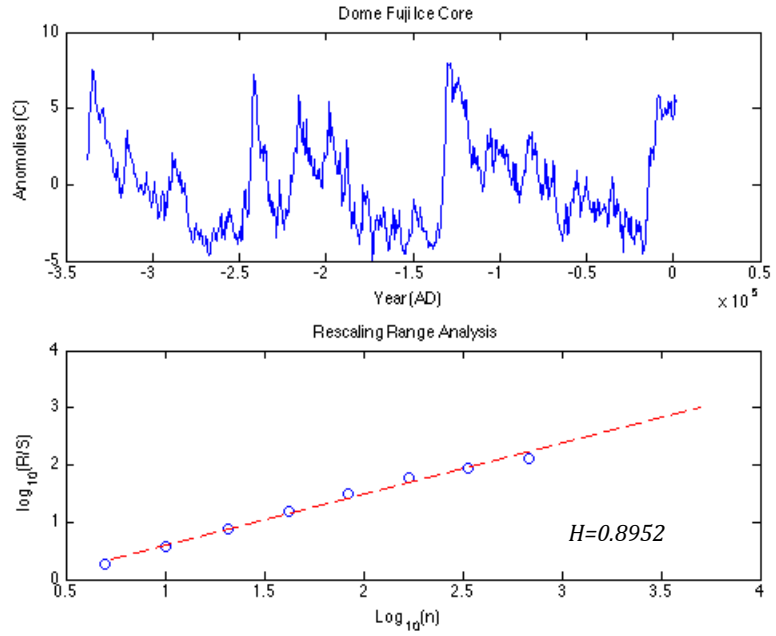

Fig. 55. Top panel: Dome Fuji, Antarctica ice core proxy temperature record. Bottom panel: log(R/S) versus log(n) rescaling range analysis show temperature records is fractal.

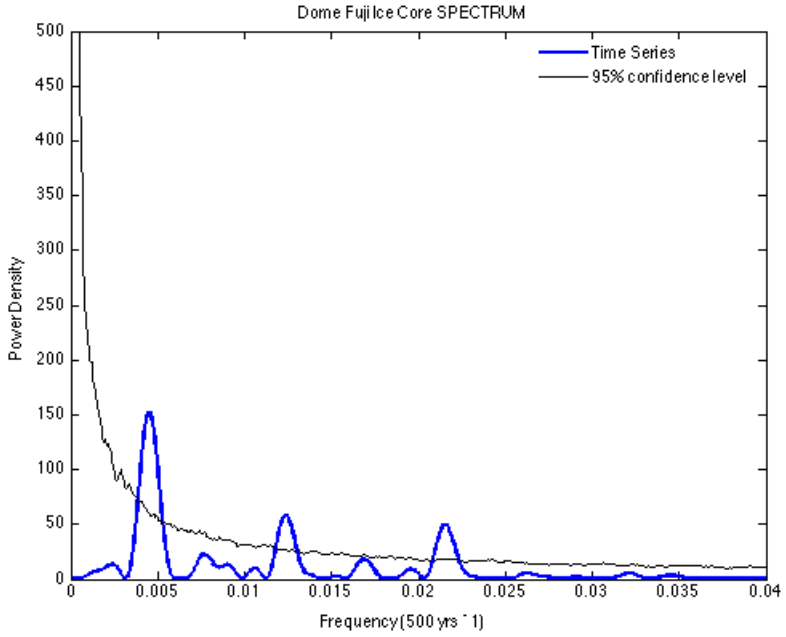

Fig. 56. Power spectrum analysis using DFT of Dome Fuji, Antarctica ice core proxy temperature record (blue) with the 95% confidence level using 1000 Monte Carlo simulations (black).

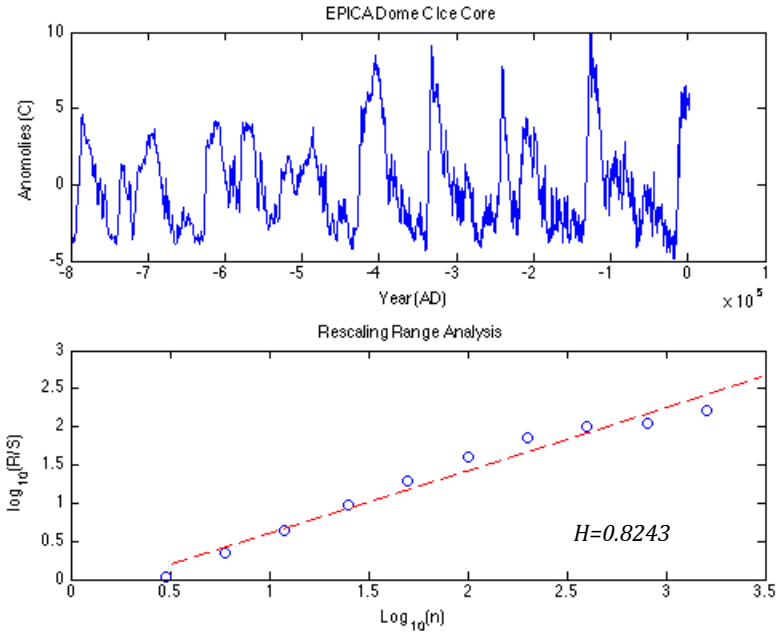

Fig. 57. Top panel: EPICA Dome C, Antarctica ice core proxy temperature record. Bottom panel: log(R/S) versus log(n) rescaling range analysis show temperature records is fractal.

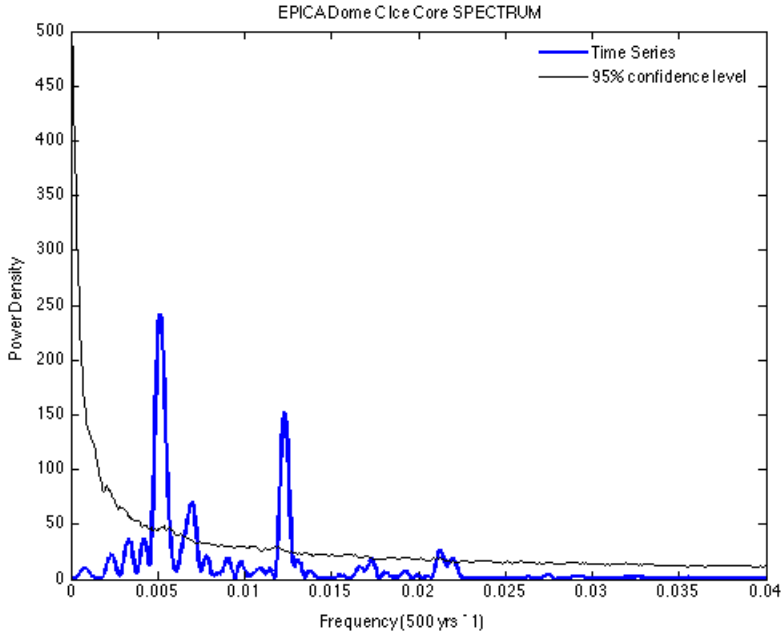

Fig. 58. Power spectrum analysis using DFT of EPICA Dome C, Antarctica ice core proxy temperature record (blue) with the 95% confidence level using 1000 Monte Carlo simulations (black).

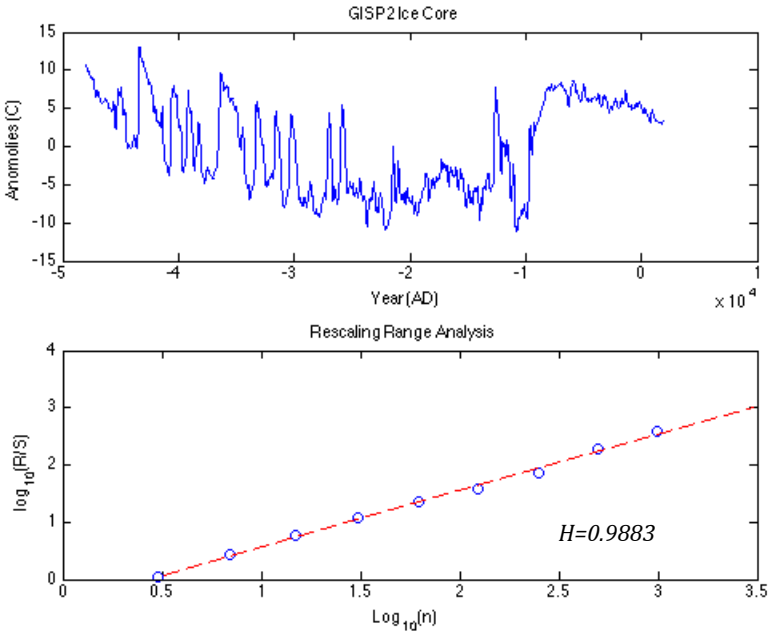

Fig. 59. Top panel: GISP2, Central Greenland ice core proxy temperature record. Bottom panel: log(R/S) versus log(n) rescaling range analysis show temperature records is fractal.

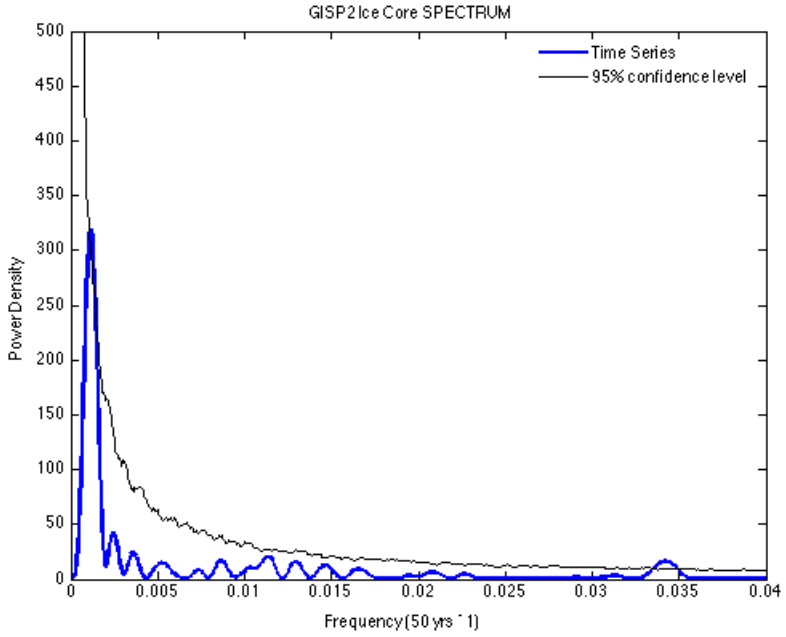

Fig. 60. Power spectrum analysis using DFT of S GISP2, Central Greenland ice core temperature record (blue) with the 95% confidence level using 1000 Monte Carlo simulations (black).

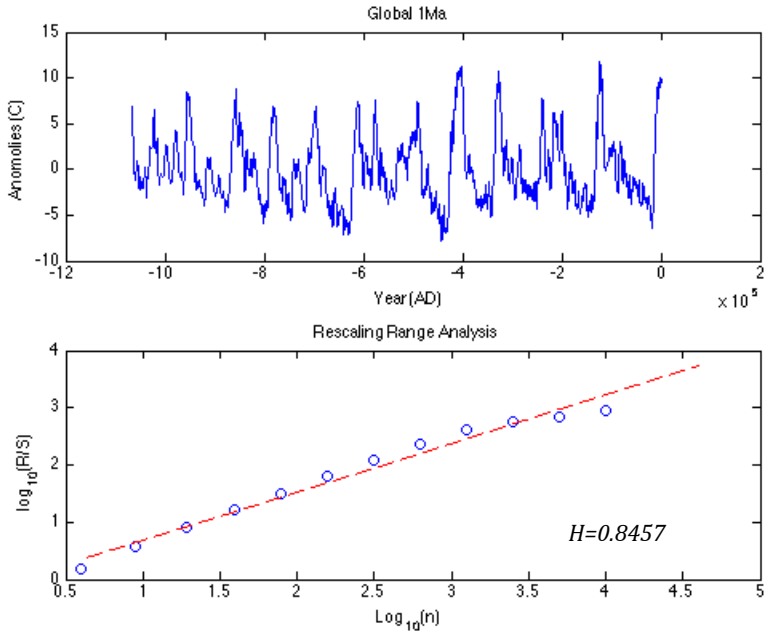

Fig. 61. Top panel: Global 1Ma proxy temperature record. Bottom panel: log(R/S) versus log(n) rescaling range analysis show temperature records is fractal.

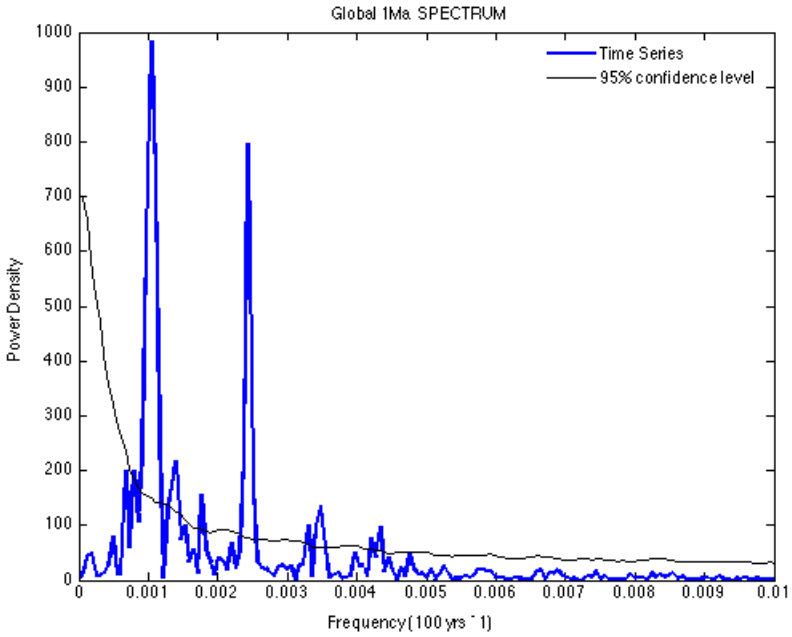

Fig. 62. Power spectrum analysis using DFT of Global 1Ma proxy temperature record (blue) with the 95% confidence level using 1000 Monte Carlo simulations (black).

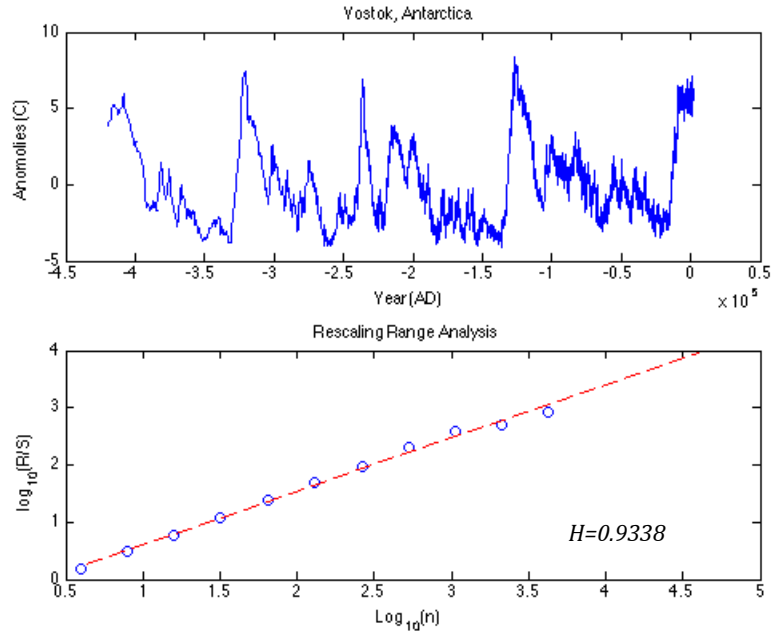

Fig. 63. Top panel: Vostok, Antarctica, ice core proxy temperature record. Bottom panel: log(R/S) versus log(n) rescaling range analysis show temperature records is fractal.

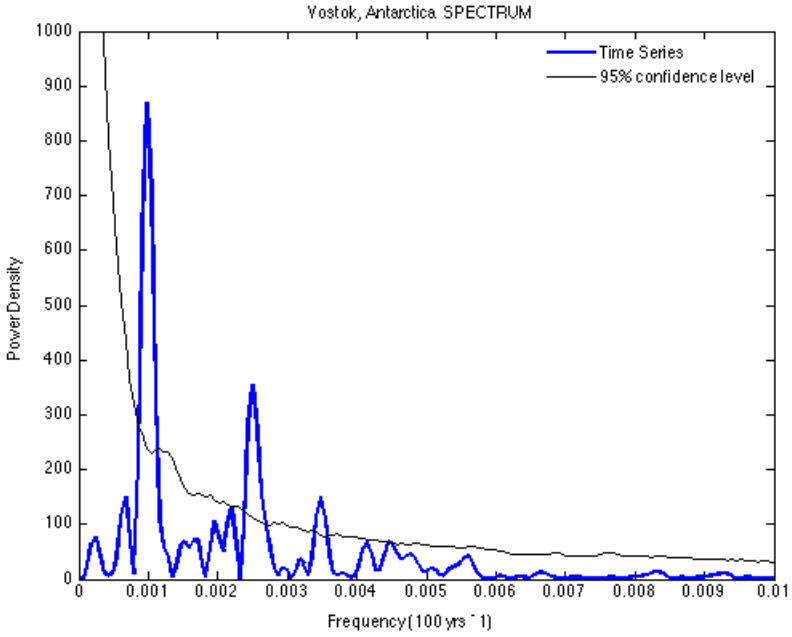

Fig. 64. Power spectrum analysis using DFT of Vostok, Antarctica, ice core proxy temperature record (blue) with the 95% confidence level using 1000 Monte Carlo simulations (black).

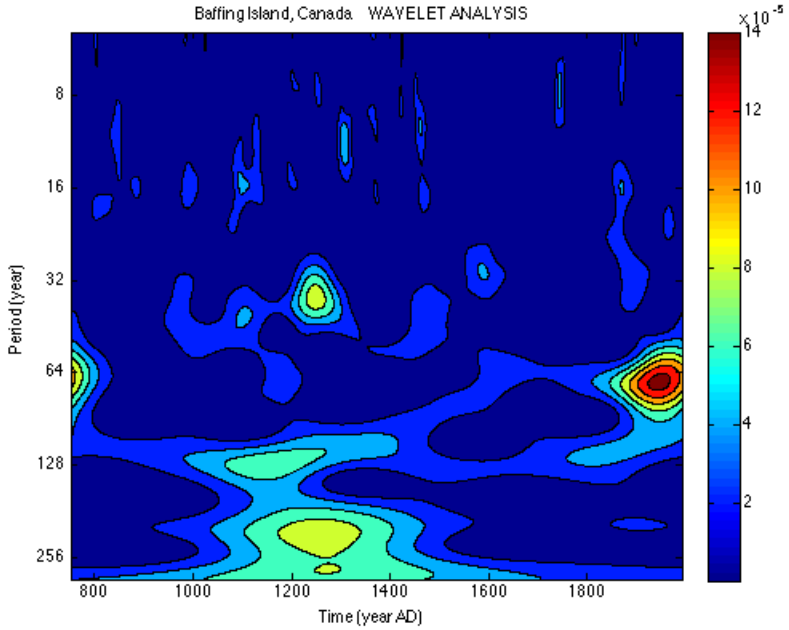

Fig. 65. Wavelet analysis of Baffin Island, Canada proxy temperature record.

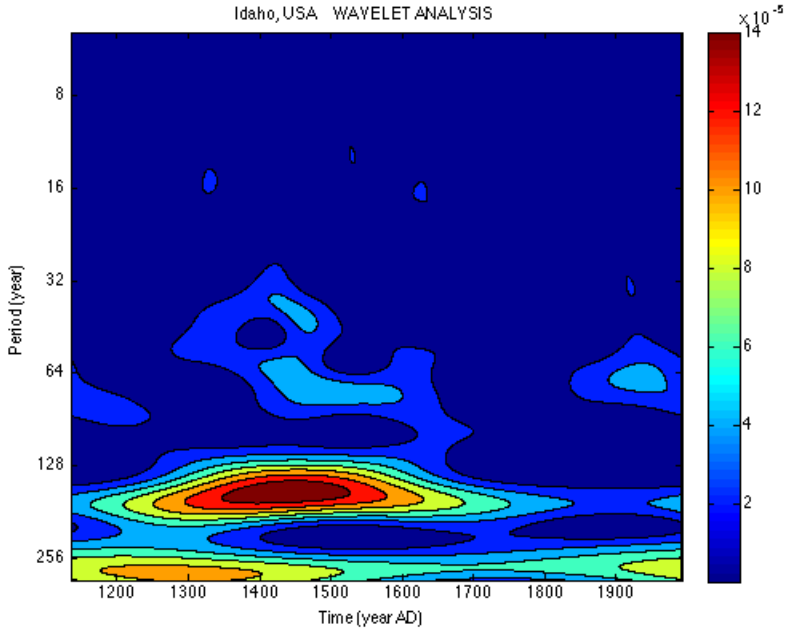

Fig. 66. Wavelet analysis of Idaho, USA proxy temperature record.

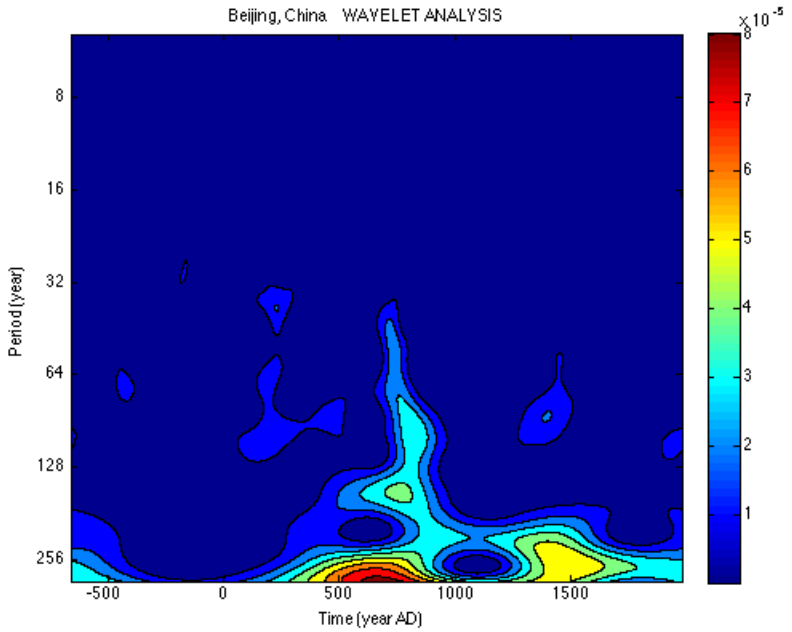

Fig. 67. Wavelet analysis of Beijing, China proxy temperature record.

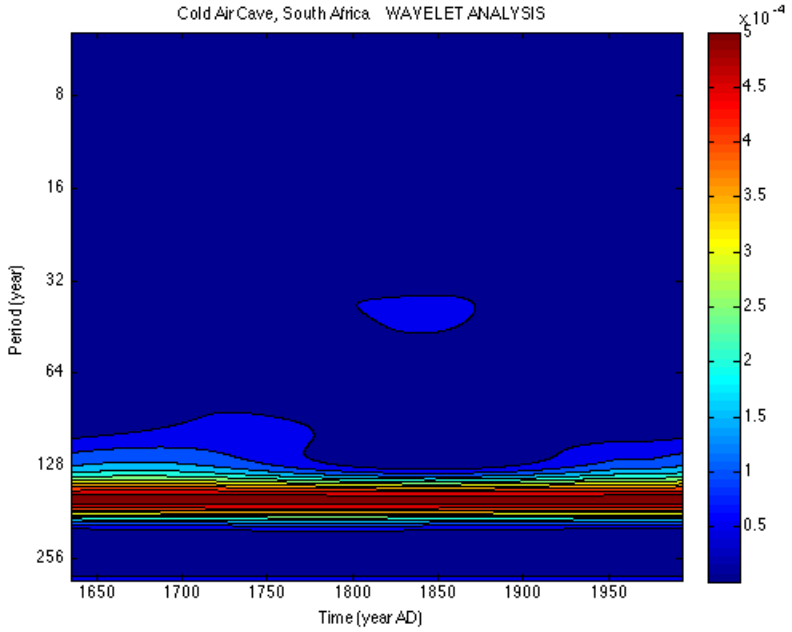

Fig. 68. Wavelet analysis of Cold Air Cave, South Africa proxy temperature record.

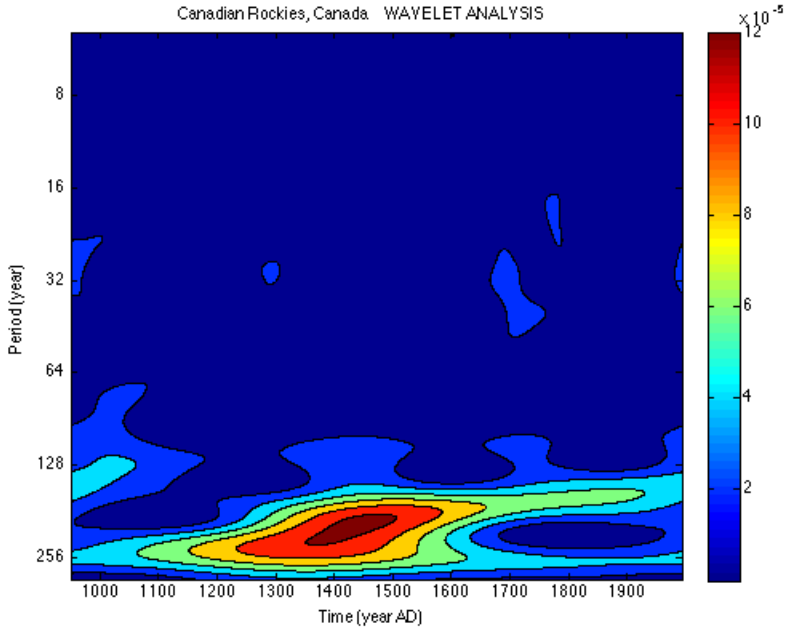

Fig. 69. Wavelet analysis of Canadian Rockies proxy temperature record.

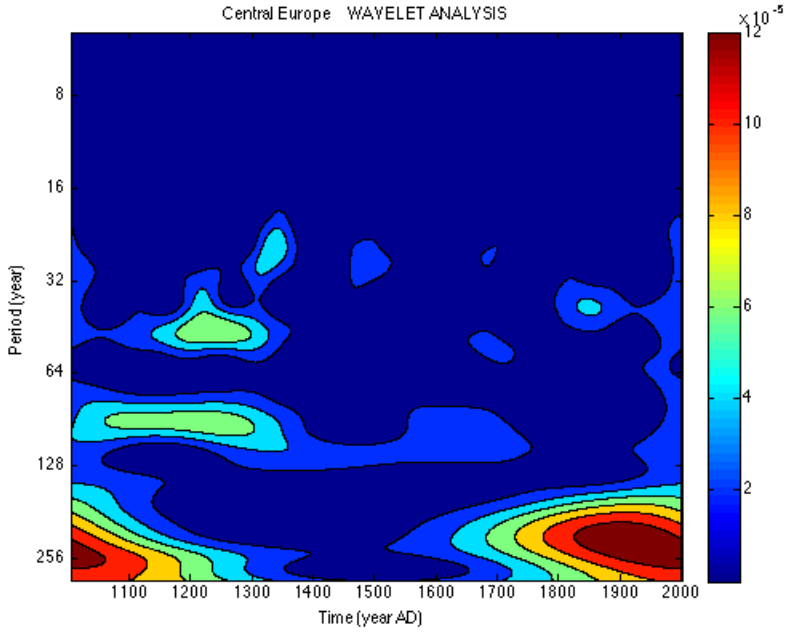

Fig. 70. Wavelet analysis of Central Europe proxy temperature record.

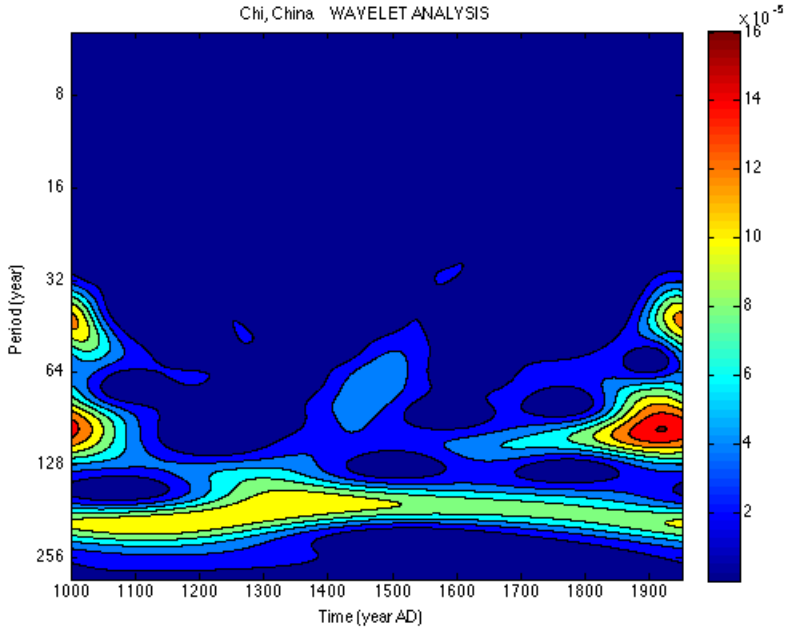

Fig. 71. Wavelet analysis of Chi, China proxy temperature record.

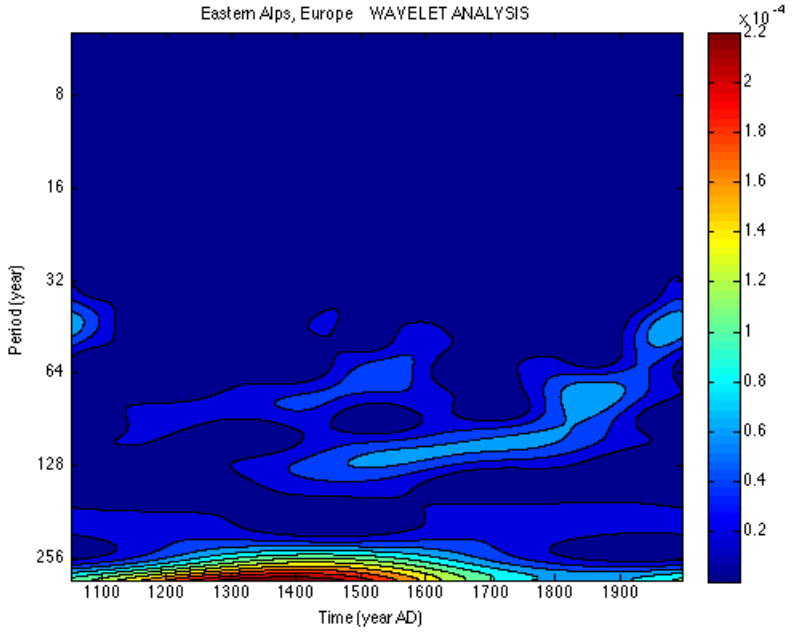

Fig. 72. Wavelet analysis of Eastern Alps, Europe proxy temperature record.

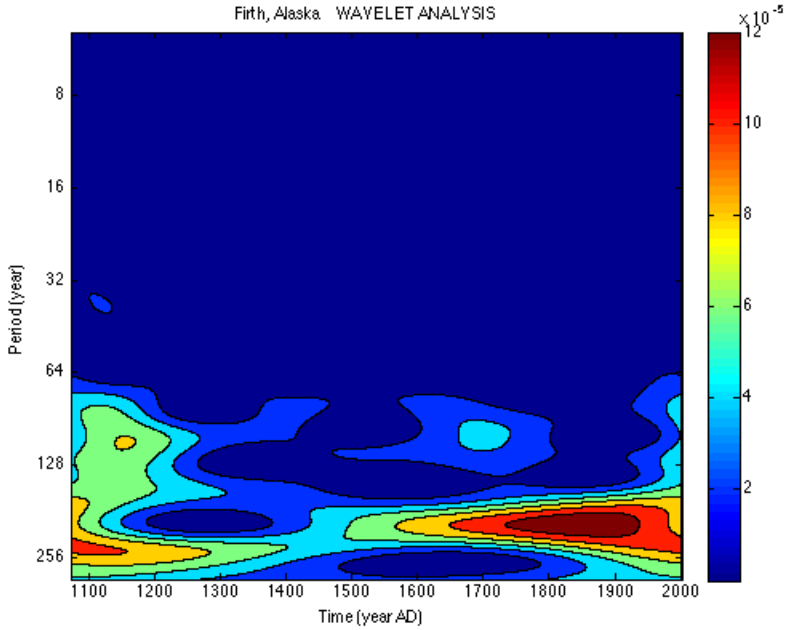

Fig.73. Wavelet analysis of Firth, Alaska proxy temperature record.

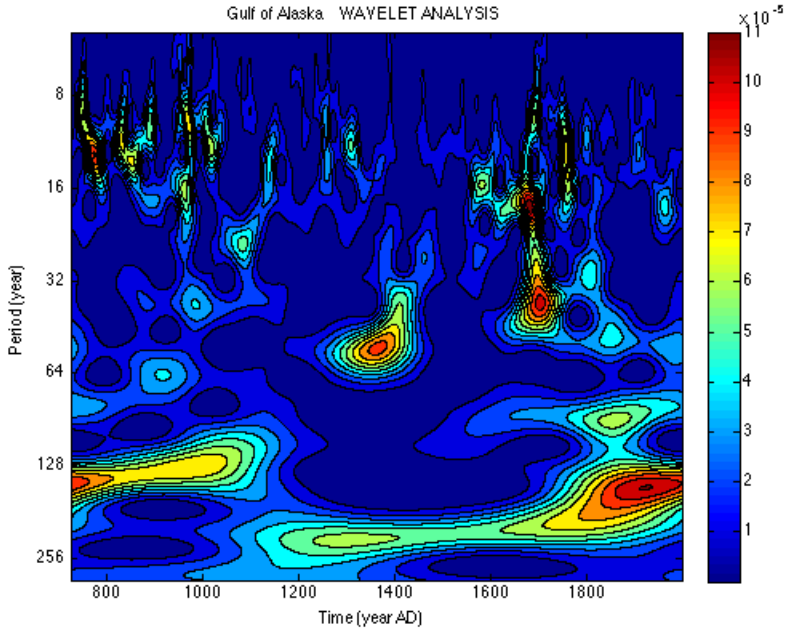

Fig. 74. Wavelet analysis of Gulf of Alaska proxy temperature record.

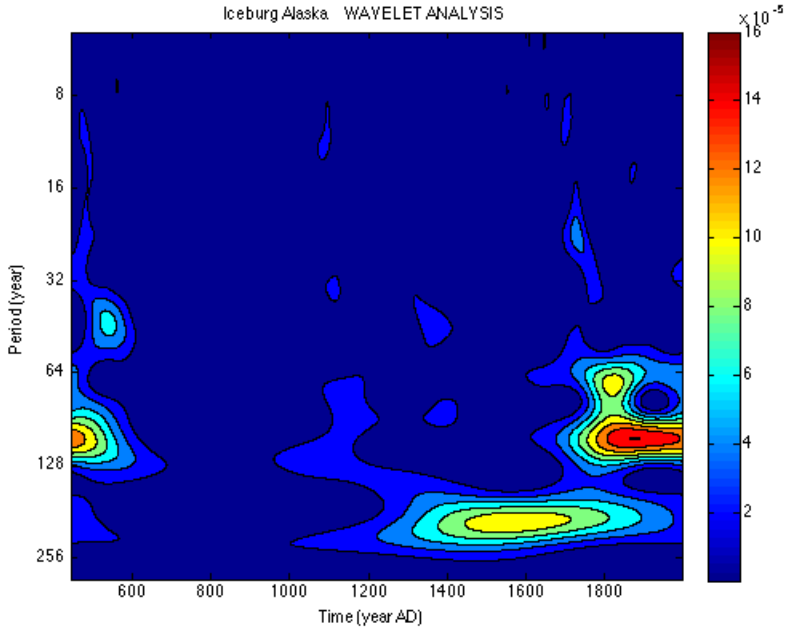

Fig. 75. Wavelet analysis of Iceberg, Alaska proxy temperature record.

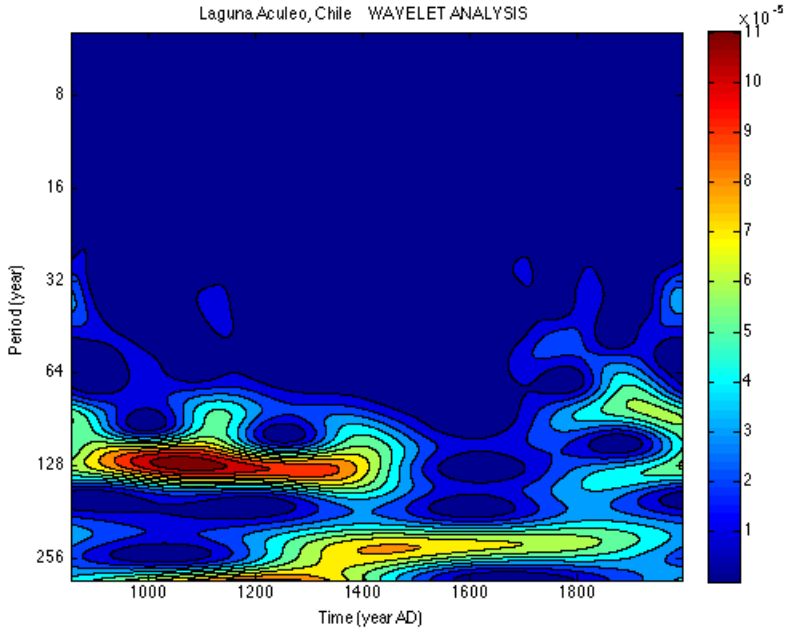

Fig. 76. Wavelet analysis of Laguna Aculeo, Chile proxy temperature record.

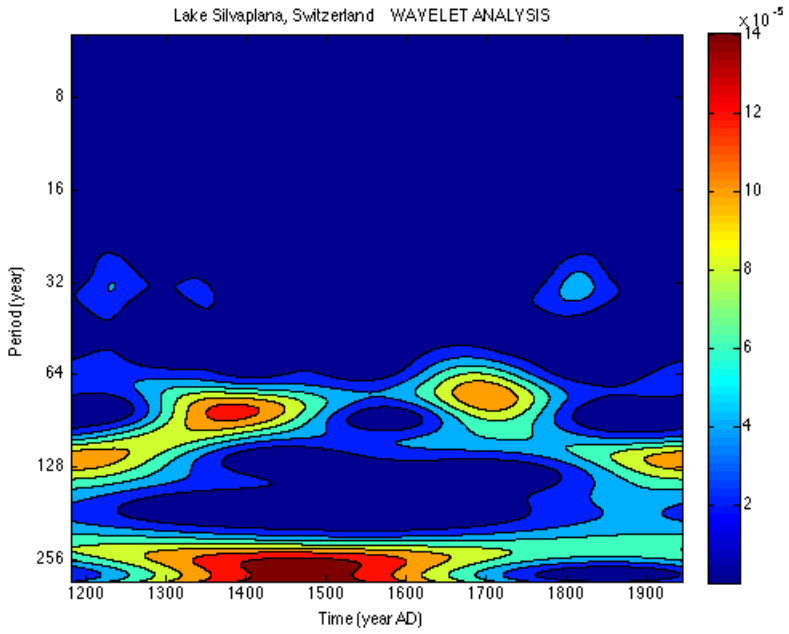

Fig. 77. Wavelet analysis of Lake Silvaplana, Switzerland proxy temperature record.

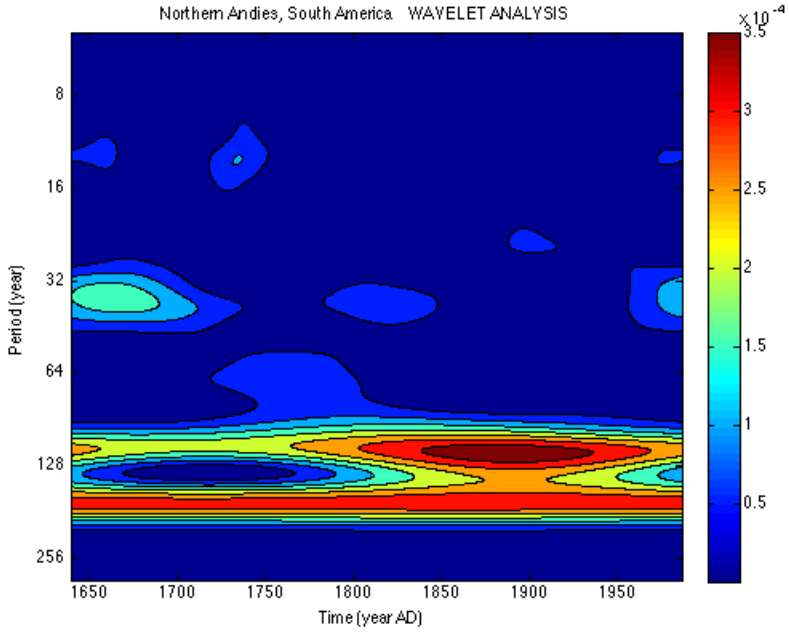

Fig. 78. Wavelet analysis of Northern Andes, South America proxy temperature record.

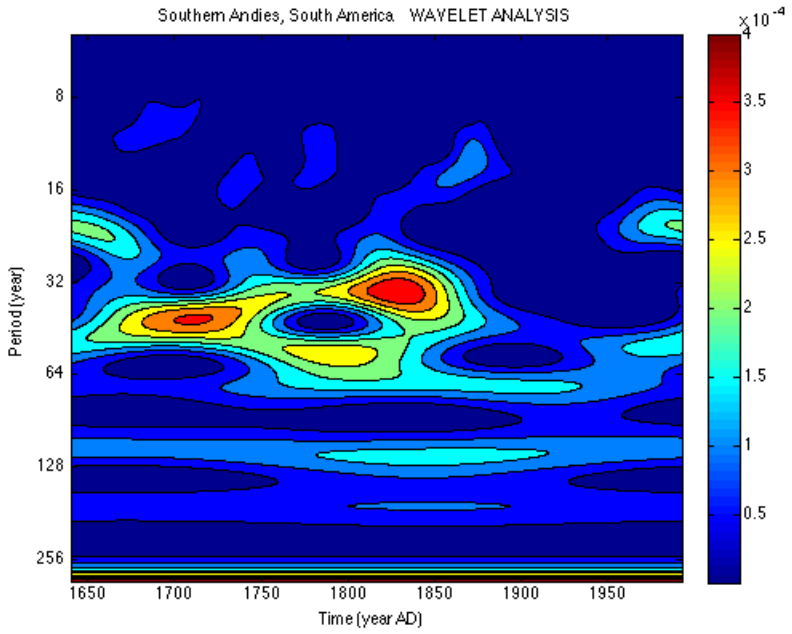

Fig. 79. Wavelet analysis of Southern Andes, South America proxy temperature record.

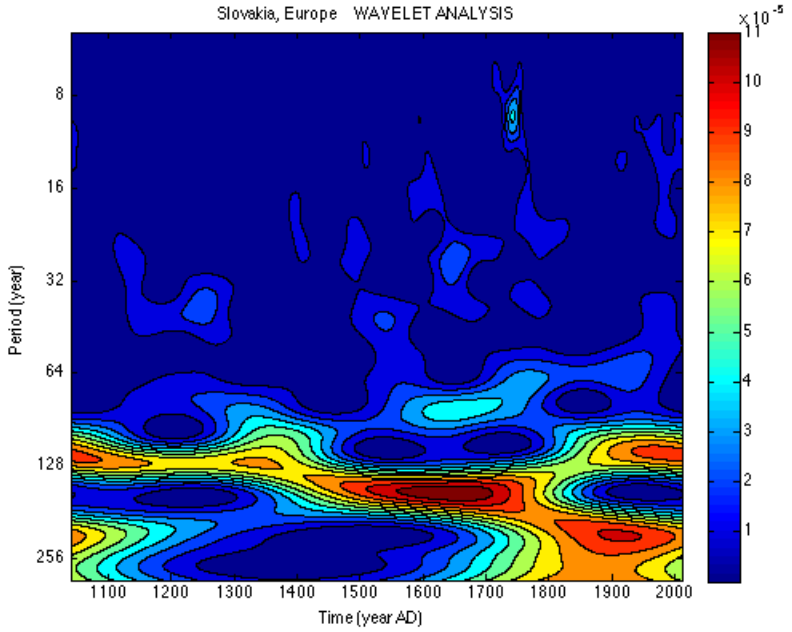

Fig. 80. Wavelet analysis of Slovakia, Europe proxy temperature record.

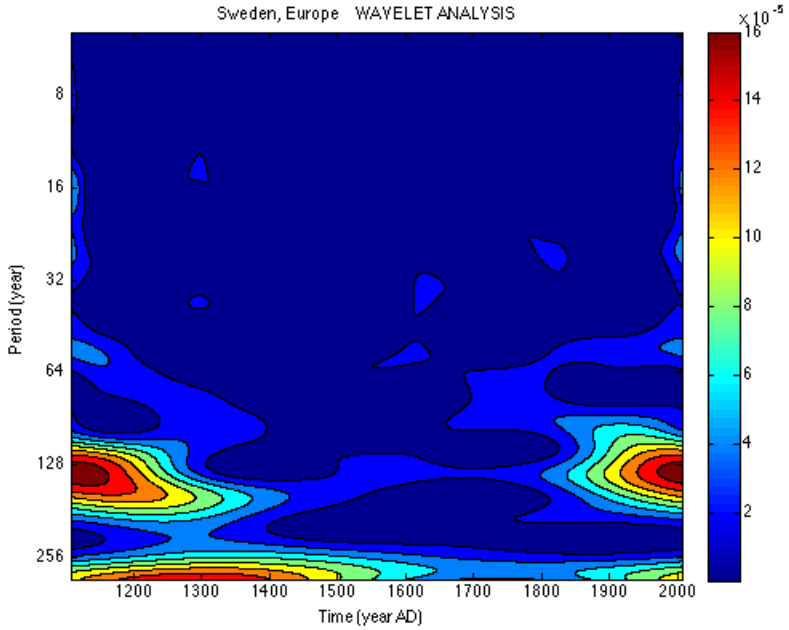

Fig. 81. Wavelet analysis of Sweden, Europe proxy temperature record.

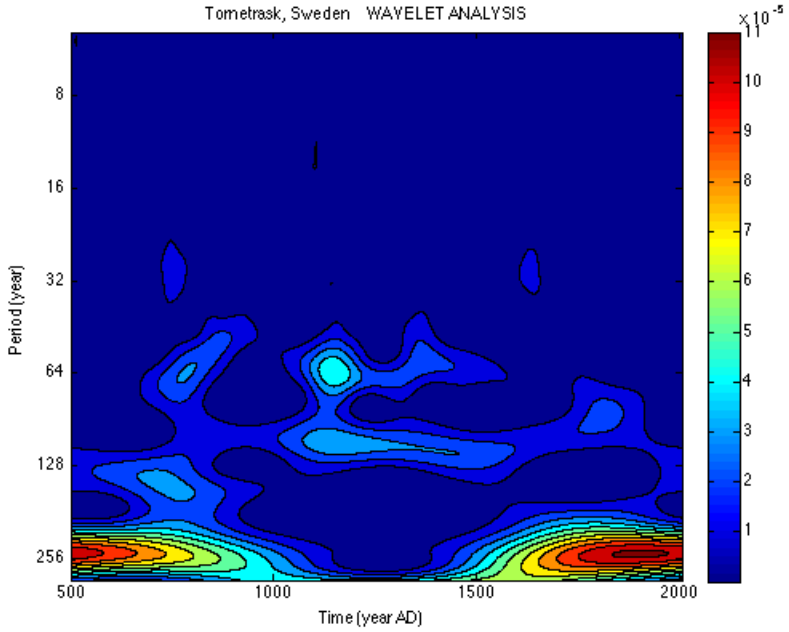

Fig. 82. Wavelet analysis of Tornetrask, Sweden proxy temperature record.

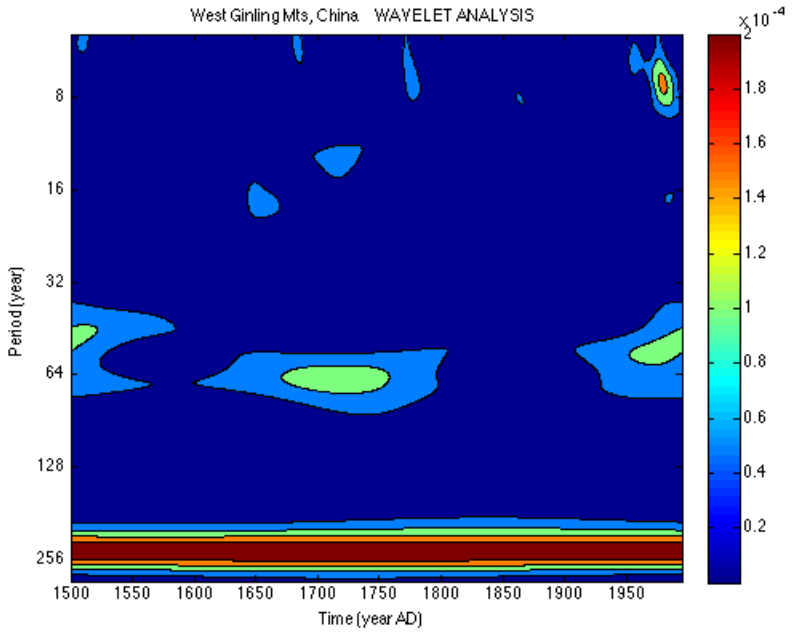

Fig. 83. Wavelet analysis of West Qinling Mts, China proxy temperature record.

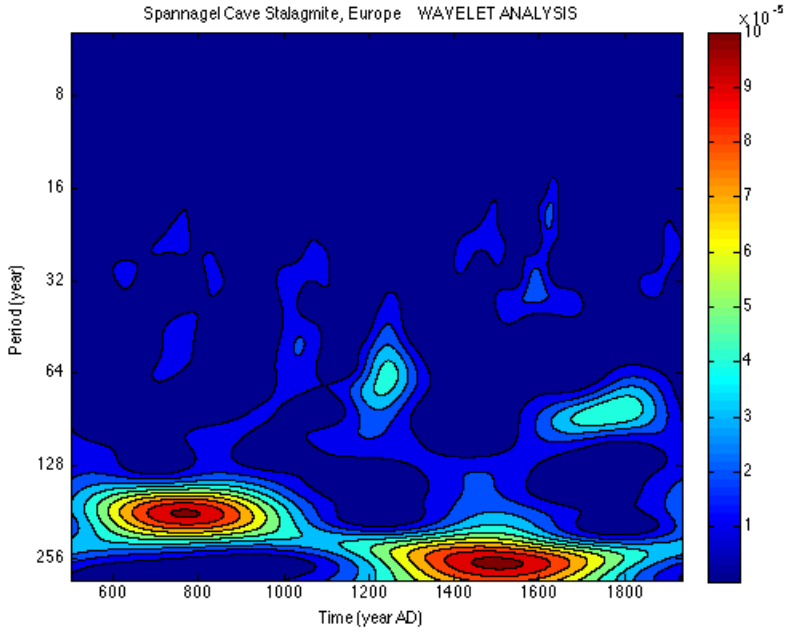

Fig. 84. Wavelet analysis of Spannagel Cave, Europe proxy temperature record.

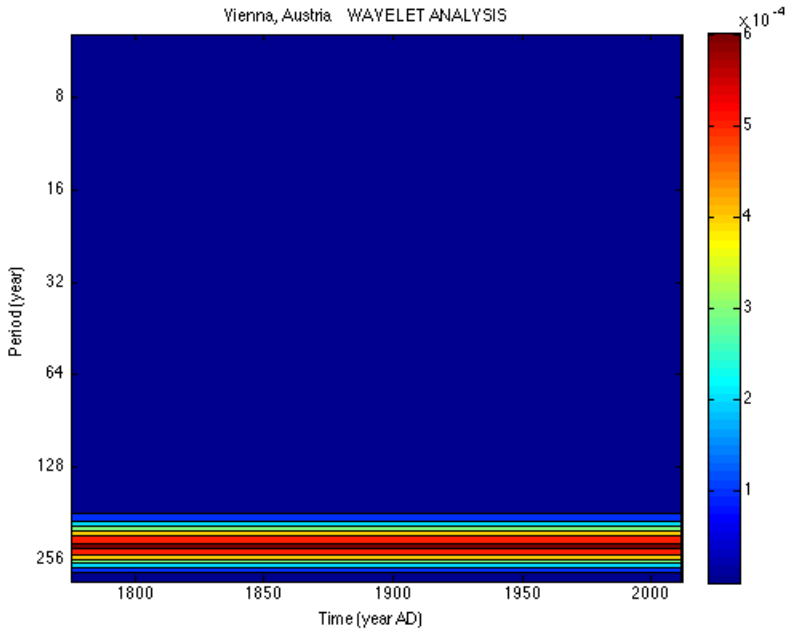

Fig.85. Wavelet analysis of Vienna, Austria instrumental temperature record.

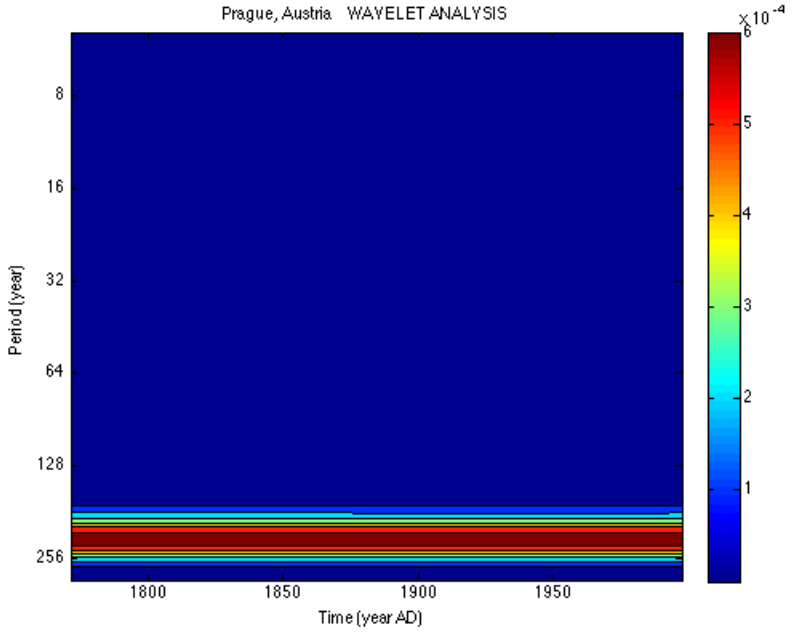

Fig.86. Wavelet analysis of Prague, Czech Republic instrumental temperature record.

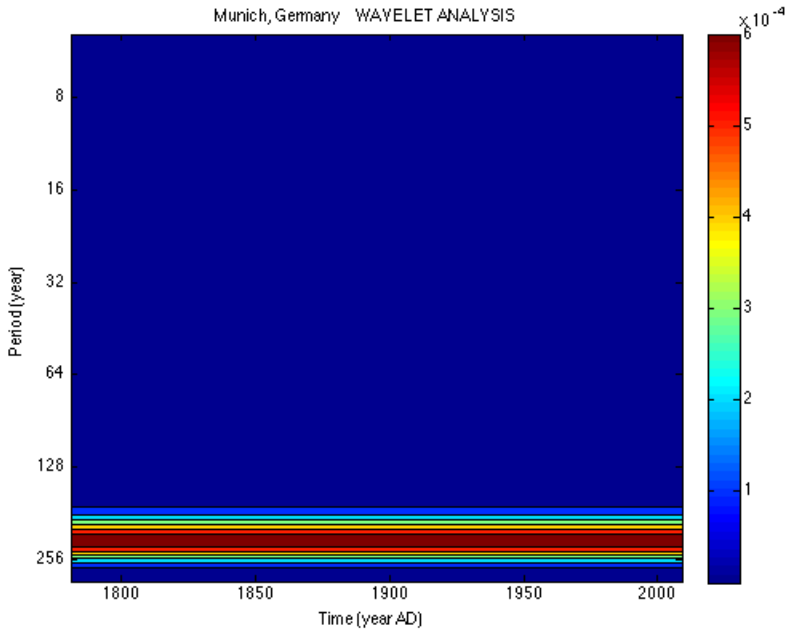

Fig.87. Wavelet analysis of Munich, Germany instrumental temperature record.

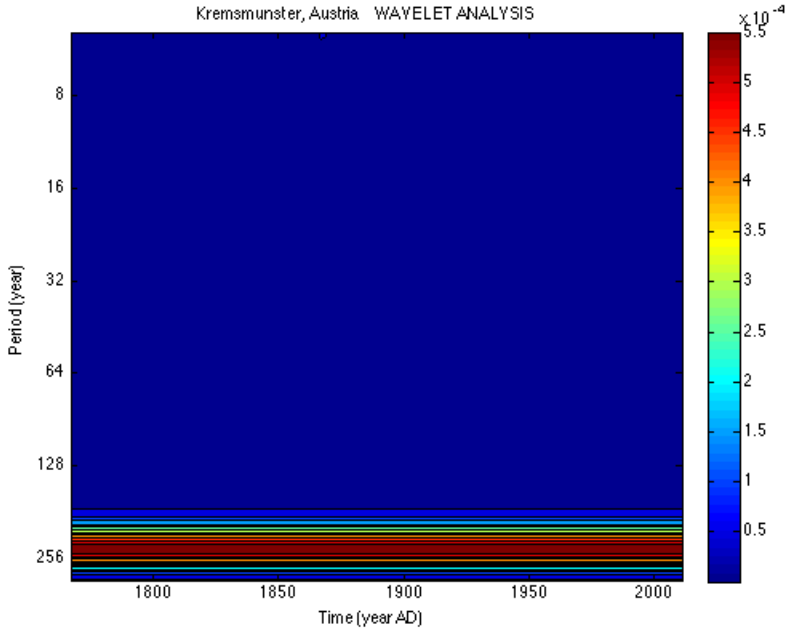

Fig.88. Wavelet analysis of Kremsmunster, Austria instrumental temperature record.

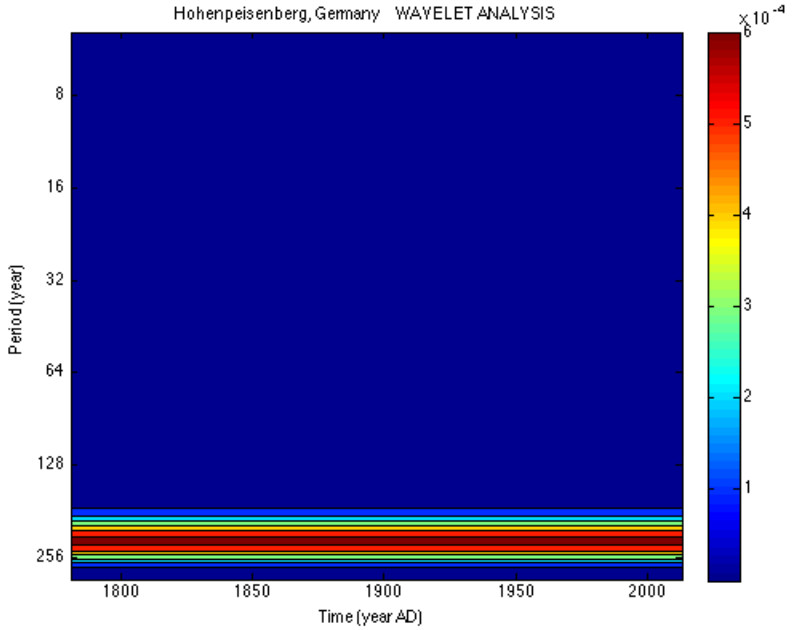

Fig.89. Wavelet analysis of Hohenpeisenberg, Germany instrumental temperature record.

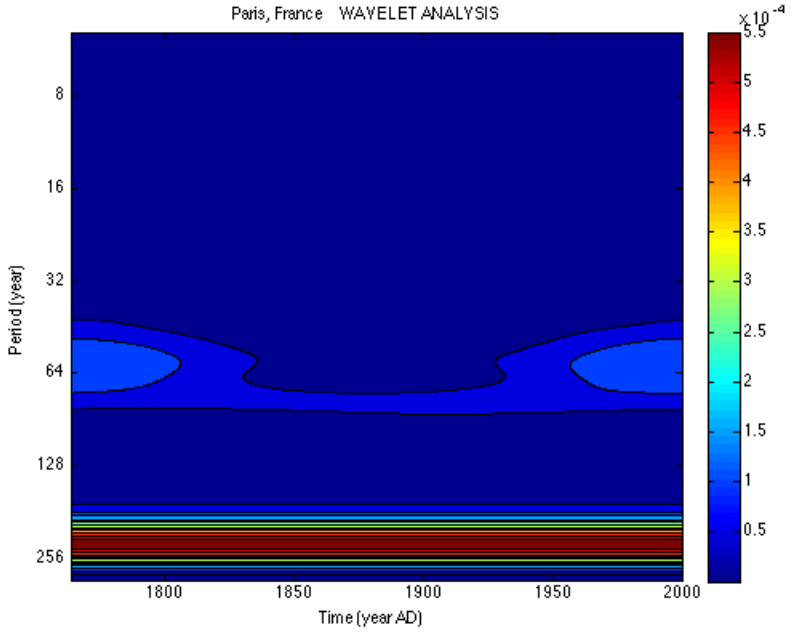

Fig.90. Wavelet analysis of Paris, France instrumental temperature record.

VIII. Table

#	Location/Name	Length	Spacing	Type	Hurst (H)
1	Laguna Aculeo, Chile	856–1997 AD	Annually	Sediment Pigments	0.9653
2	Baffin Island, Canada	752–1992 AD	Annually	Sediment Thickness	0.7261
3	Canadian Rockies	950–1994 AD	Annually	Tree-Ring Thickness	0.8428
4	Firth, Alaska	1073–2002 AD	Annually	Tree-Ring Thickness	0.9156
5	Iceberg, Alaska	442–1998 AD	Annually	Varve Thickness	0.6611
6	Gulf of Alaska	724–1999 AD	Annually	Tree-Ring Thickness	0.8278
7	Idaho, USA	1135–1992 AD	Annually	Tree-Ring Thickness	0.8300
8	Northern Andes, South America	1640–1987 AD	Annually	Tree-Ring Thickness	0.8549
9	Southern Andes, South America	1640–1993 AD	Annually	Tree-Ring Thickness	0.7972
10	Beijing, China	-665–1985 AD	Annually	Stalagmite Thickness	0.8551
11	Central Europe	1005–2001 AD	Annually	Documentary Data	0.8945
12	China	1000–1950 AD	Annually	Multi-Proxy Reconstruction	0.9365
13	Cold Air Cave, South Africa	1635–1993 AD	Annually	Stalagmite Isotope	0.9269
14	Eastern Alps, Europe	1053–1996 AD	Annually	Tree-Ring and Sediment Thickness	0.9775
15	Lake Silvaplana, Switzerland	1175–1949 AD	Annually	Spectroscopy of Lake Sediment	0.9197
16	Slovakia, Europe	1040–2011 AD	Annually	Tree-Ring Thickness	0.8675
17	Sweden, Europe	1107–2007 AD	Annually	Tree-Ring Thickness	0.9123
18	Tornetrask, Sweden	500–2004 AD	Annually	Tree-Ring Thickness	0.8774
19	West Qinling Mts., China	1500–1995 AD	Annually	Tree-Ring Thickness	0.7611
20	Paris, France	1764–2000 AD	Monthly	Instrumental Records	0.8498
21	Hohenpeisenberg, Germany	1781–2013 AD	Monthly	Instrumental Records	0.8570
22	Kremamunster, Austria	1767–2013 AD	Monthly	Instrumental Records	0.8559
23	Munich, Germany	1781–2011 AD	Monthly	Instrumental Records	0.8701
24	Prague, Czech Republic	1771–2013 AD	Monthly	Instrumental Records	0.8585
25	Vienna, Austria	1775–2013 AD	Monthly	Instrumental Records	0.8626
26	Spannagel Cave, Europe	-9–1935 AD	Uneven	Stalagmite thickness	0.9908
27	Dome Fuji, Antarctica	-339500–750 AD	500 yrs.	Ice Core Samples	0.8952
28	EPICA Dome C, Antarctica	-800,000–1900 AD	Uneven	Ice Core Samples	0.8243
29	GISP2, Central Greenland	-48000–1850 AD	Uneven	Ice Core Samples	0.9883
30	Global 1Ma,	-1067900–2000 AD	500 yrs.	Marine Benthic Oxygen Isotopes	0.8457
31	Vostok, Antarctica	-470766–2000 AD	Uneven	Ice Core Samples	0.9338

Table 1: Table of all Data used within this study including location/name, length, time spacing and type of proxy/instrumental records.

IX. Reference:

Alley, R.B.. 2004. GISP2 Ice Core Temperature and Accumulation Data. IGBP PAGES/World Data Center for Paleoclimatology Data Contribution Series #2004-013. NOAA/NGDC Paleoclimatology Program, Boulder CO, USA.

Anchukaitis, Kevin J.; D'Arrigo, Rosanne D.; Andreu-Hayles, Laia; Frank, David; Verstege, Anne; Curtis, Ashley; Buckley, Brendan M.; Jacoby, Gordon C.; Cook, Edward R. 2013. Tree-Ring-Reconstructed Summer Temperatures from Northwestern North America during the Last Nine Centuries. Journal of Climate, Vol. 26 Number 10, pp. 3001-3012. DOI: 10.1175/JCLI-D-11-00139.1

Auer, I., Bohm, R., Jurkovic, A., Lipa, W., Orlik, A., Potzmann, R., Schoner, W., Ungersbock, M., Matulla, C., Briffa, K., Jones, P., Efthymiadis, D., Brunetti, M., Nanni, T., Maugeri, M., Mercalli, L., Mestre, O., Moisselin, J.-M., Begert, M., Muller-Westermeier, G., Kveton, V., Bochnicek, O., Stastny, P., Lapin, M., Szalai, S., Szentimrey, T., Cegnar, T., Dolinar, M., Gajik-Capka, M., Zaninovic, K., Majstorovic, Z., and Nieplova, E.:HISTALP – historical instrumental climatological surface time series of the Greater Alpine Region, Int. J. Climatol., 27, 17–46, 2007.

Bintanja, R., R.S.W. van de Wal, and J. Oerlemans. 2005. Modelled atmospheric temperatures and global sea levels over the past million years. Nature, Vol. 437, pp. 125-128, 1 September 2005. doi:10.1038/nature03975

Biondi, F., et al. 2006. East-central Idaho July Temperature Reconstruction. IGBP PAGES/World Data Center for Paleoclimatology Data Contribution Series # 2006-039. NOAA/NCDC Paleoclimatology Program, Boulder CO, USA.

Büntgen, Ulf; Kyncl, Tomás; Ginzler, Christian; Jacks, David S.; Esper, Jan; Tegel, Willy; Heussner, Karl-Uwe; and Kyncl, Josef. 2013. Filling the Eastern European gap in millennium-long temperature reconstructions. Proceedings of the National Academy of Sciences, January 2013. DOI: 10.1073/pnas.1211485110

Climate Research Unit (CRU): University of East Anglia (UK), Available at: http://www.metoffice.gov.uk/hadobs/crutem4/data/download.html (last access: June 2014), 2014

Czech Hydrometeorological Institute (CHMI): 143 06 Praha 4 Czech Republic, available at: http://zmeny-klima.ic.cz/klementinum-data/ (last access: June 2014), 2012

Deutscher Wetterdienst (DWD): Frankfurter Straße 135, 63067 Offenbach (Germany), available at: www.dwd.de (last access: June 2014), 2012

Feder, Jens. Fractals. New York: Plenum Press, 1988. . Print.

Feigenbaum, M. J.: Quantitative universality for a class of nonlinear transformations, J. Stat. Phys., 19, 25–51, 1978.

Feigenbaum, M. J.: Universal behavior in nonlinear systems, Physica D, 7, 16–39, 1983.

Glaser, R. and Riemann, D. 2009. A thousand-year record of temperature variations for Germany and Central Europe based on documentary data. Journal of Quaternary Science, Vol. 24, pp. 437-449. ISSN 0267-8179. DOI: 10.1002/jqs.1302

Grudd, H. 2008. Tornetrask tree-ring width and density AD 500-2004: a test of climatic sensitivity and a new 1500-year reconstruction of north Fennoscandian summers. Climate Dynamics, Vol. 31, pp. 843-857. DOI:10.1007/s00382-007-0358-2

Gunnarson, Björn E.; Linderholm, Hans W.; Moberg, Anders. January 2011. Improving a tree-ring reconstruction from west-central Scandinavia: 900 years of warm-season temperatures. Climate Dynamics, Vol. 36, No. 1-2, pp. 97-108, January 2011. DOI: 10.1007/s00382-010-0783-5

Jouzel, J., et al. 2007. EPICA Dome C Ice Core 800KYr Deuterium Data and Temperature Estimates. IGBP PAGES/World Data Center for Paleoclimatology Data Contribution Series # 2007-091. NOAA/NCDC Paleoclimatology Program, Boulder CO, USA.

Kawamura, K., et al. 2007. Dome Fuji Ice Core Preliminary Temperature Reconstruction, 0-340 kyr. IGBP PAGES/World Data Center for Paleoclimatology Data Contribution Series # 2007-074. NOAA/NCDC Paleoclimatology Program, Boulder CO, USA.

Loso, M.G. 2008. Summer temperatures during the Medieval Warm Period and Little Ice Age inferred from varved proglacial lake sediments in southern Alaska. Journal of Paleolimnology, Vol. 41, No. 1, pp. 117-128, January 2009. doi: 10.1007/s10933-008-9264-9

Luckman, B.H. and R.J.S. Wilson. 2006. Canadian Rockies Summer Temperature Reconstruction. IGBP PAGES/World Data Center for Paleoclimatology Data Contribution Series # 2006-011. NOAA/NCDC Paleoclimatology Program, Boulder CO, USA. CONTRIBUTORS: Brian Luckman, University of Western Ontario, and Rob Wilson, Edinburgh University.

Lüdecke, H.-J., Hempelmann, A., Weiss, C. O.: Multi-periodic climate dynamics: spectral analysis of long-term instrumental and proxy temperature records. Clim. Past, 9, 447–452, 2013.

Mangini, A., C. Spötl, and P. Verdes. 2005. Reconstruction of temperature in the Central Alps during the past 2000 yr from a d18O stalagmite record. Earth and Planetary Science Letters, Vol. 235, Issues 3-4, Pages 741-751, 15 July 2005. doi:10.1016/j.epsl.2005.05.010

MATLAB and Statistics Toolbox Release 2012b, The MathWorks, Inc., Natick, Massachusetts, United States. Last accessed June 2014.

Météo France: available at: http://france.meteofrance.com. access: June 2014), 42 Av. Gaspard Coriolis, 31057 Toulouse Cedex (France), 2012.

Moore, J.J., et al., 2003, Baffin Island 1250 Year Summer Temperature Reconstruction, IGBP PAGES/World Data Center for Paleoclimatology Data Contribution Series # 2003-075. NOAA/NGDC Paleoclimatology Program, Boulder CO, USA. CONTRIBUTOR: Konrad Hughen, University of Colorado (now at Woods Hole Oceanographic Institution)

Petit J.R., Jouzel J., Raynaud D., Barkov N.I., Barnola J.M., Basile I., Bender M., Chappellaz J., Davis J., Delaygue G., Delmotte M., Kotlyakov V.M., Legrand M., Lipenkov V., Lorius C., PÈpin L., Ritz C., Saltzman E., Stievenard M., 1999, Climate and Atmospheric History of the Past 420,000 years from the Vostok Ice Core, Antarctica, Nature, 399, pp.429-436.

Schulz, M. and Mudelsee, M.: REDFIT: estimating red-noise spectra directly from unevenly spaced paleoclimatic time series, Comput. Geosci., 28, 421–426, 2002.

Shi, Feng; Yang, Bao; and Von Gunten, Lucien. 2012. Preliminary multiproxy surface air temperature field reconstruction for China over the past millennium. Science China Earth Sciences, Vol. 55, No. 12, pp. 2058-2067, December 2012. DOI: 10.1007/s11430-012-4374-7

Sundqvist, H.S.; Holmgren, K.; Fohlmeister, J.; Zhang, Q.; Bar Matthews, M.; Spitl, C.; and Kirnich, H. 2013. Evidence of a large cooling between 1690 and 1740 AD in southern Africa. Scientific Reports, Vol 3, No. 1767, May 2013. DOI: 10.1038/srep01767

Tan, M., et al., 2003, 2650-Year Beijing Stalagmite Layer Thickness and Temperature Reconstruction, IGBP PAGES/World Data Center for Paleoclimatology Data Contribution Series # 2003-050. NOAA/NGDC Paleoclimatology Program, Boulder CO, USA.

Trachsel, M., C. Kamenik, M. Grosjean, D. McCarroll, A. Moberg, R. Br·zdil, U. B¸ntgen, P. Dobrovoln˝, J. Esper, D.C. Frank, M. Friedrich, R. Glaser, I. Larocque-Tobler, K. Nicolussi, and D. Riemann. 2012. Multi-archive summer temperature reconstruction for the European Alps, AD 1053-1996. Quaternary Science Reviews, Vol. 46, pp. 66-79. doi:10.1016/j.quascirev.2012.04.021

Trachsel, M., M. Grosjean, D. Schnyder, C. Kamenik, and B. Rein. 2010. Scanning reflectance spectroscopy (380ñ730 nm): a novel method for quantitative high-resolution climate reconstructions from minerogenic lake sediments. Journal of Paleolimnology, December 2010, Vol. 44, Issue 4, pp 979-994. DOI: 10.1007/s10933-010-9468-7

Villalba, R., et al.. 2006. Southern Andes Temperature Reconstructions. IGBP PAGES/World Data Center for Paleoclimatology Data Contribution Series # 2006-024. NOAA/NCDC Paleoclimatology Program, Boulder CO, USA.

Von Gunten, L., M. Grosjean, B. Rein, R. Urrutia, and P. Appleby. 2009. A quantitative high-resolution summer temperature reconstruction based on sedimentary pigments from Laguna Aculeo, central Chile, back to AD 850. The Holocene, Vol. 19, Number 6, pp. 873-881. DOI: 10.1177/0959683609336573

Wilson, R., G. Wiles, R. DíArrigo, and C. Zweck. 2007. Cycles and shifts: 1,300 years of multi-decadal temperature variability in the Gulf of Alaska. Climate Dynamics, Vol. 28, pp. 425-440. DOI 10.1007/s00382-006-0194-9

Yang, Fengmei; Wang, Naiang; Shi, Feng; Ljungqvist, Fredrik Charpentier; Wang, Shigong; Fan, Zexin; Lu, Junwei. 2013. Multi-Proxy Temperature Reconstruction from the West Qinling Mountains, China, for the Past 500 Years. PLOS One, Vol. 8, No. 2, February 2013. DOI: 10.1371/journal.pone.0057638